An analytical framework for estimating drying shrinkage strain of OPC based hardened cement paste

An Analytical Framework for Estimating Drying Shrinkage Strain of OPC Based Hardened Cement Paste

Saeid Babaei[*(1)a,b,c], Suresh C. Seetharam[(2)a], Arnaud Dizier[(3)c], Gunther Steenackers[(4)b,d] and Bart Craeye[(5)b,e]

[a] Engineered and Geosystems Analysis Unit, Institute for Environment, Health, and Safety, Belgian Nuclear Research Centre (SCK•CEN), Boeretang 200, B-2400 Mol, Belgium.

[b] Faculty of Applied Engineering, University of Antwerp, EMIB Research Group, Groenenborgerlaan 171 - 2020 Antwerpen , Belgium

[c] EIG, EURIDICE, Belgian Nuclear Research Centre (SCK•CEN), Boeretang 200, B-2400 Mol, Belgium

[d] Faculty of Applied Engineering, University of Antwerp | Op3Mech Research Group Groenenborgerlaan 171 - 2020 Antwerpen

[e] Odisse University College, Industrial Services & Technologies, DUBIT Research Unit, Belgium

(1)* Tel: +32 14 333118, saeid.babaei@uantwerpen.be; saeid.babaei@sckcen.be

(2) Tel: +32 14 333208, suresh.seetharam@sckcen.be

(3) Tel: +32 14 332998, arnaud.dizier@euridice.be

(4) Tel: +32 00 000000, gunther.steenackers@uantwerpen.be

(5) Tel: +32 00 000000, bart.craeye@uantwerpen.be

ABSTRACT

A new analytical framework that relies on minimal inputs and combines a number of existing techniques to estimate reversible drying shrinkage strain of OPC-based materials is presented. This includes a multiscale framework for estimating water (de)sorption isotherm (WSI), an analytical homogenization technique to estimate bulk modulus, and a multi-mechanism based drying shrinkage formulation. The minimal inputs needed are the cement composition, microstructural information and mechanical properties of hydrated phases of hardened cement paste. A pore network model that forms the core module of the multiscale WSI provides a quantitative basis for the drying shrinkage formulation. The unique feature of the framework is that only two calibration parameters are involved: (i) a geometric parameter used in the pore network model, and (ii) a constant in the disjoining pressure relationship, which is set to unity mainly due to a lack of knowledge. Importantly, there is no need to calibrate these parameters for every experiment. Results from the framework are compared against shrinkage data from literature that encompass both virgin materials (samples that have never been dried prior to the test) and non-virgin materials. A reasonably good correspondence has been achieved with respect to the non-virgin materials, whereas, the results for the virgin materials are examined mainly to gain qualitative understanding of the role of the microstructure on irreversible deformation and thus to propose a phenomenological model.

KEYWORDS

Hardened cement paste, Drying shrinkage, Poroelasticity, Disjoining pressure, Surface free energy, Multi-mechanism shrinkage, Homogenization, Multiscale

1 INTRODUCTION

For massive civil engineering concrete structures, the drying shrinkage strain is usually neglected because water exchange with the surrounding environment is very slow and mostly its effect such as cracking is limited to a thin outer layer of the structure [1]. Moreover, in massive structures, peak temperature due to heat of hydration remains only for a few days thus limiting any adverse effect on drying rate [2]. However, this may not necessarily be the case in applications related to massive non-reinforced concrete engineered barriers for deep geological disposal of radioactive waste [3, 4]. In particular, the so-called Supercontainer concept currently under consideration in Belgium, encapsulates within a concrete buffer, high-level radioactive waste (HLW) materials that release decay heat over hundreds of years. Depending on the type of waste, temperatures can reach 100 ºC at the interface between the HLW canisters and concrete buffet [5], with an increased tendency to initiate a severe drying front at the interface and further into outer layers of the buffer. Therefore, the knowledge of drying shrinkage strain in the entire relative humidity (h) range becomes necessary. This is in addition to the contribution from other eigenstrains such as thermal and creep strains. In such applications, optimum choice of cement formulation at the design phase is essential and hence *a priori* knowledge of drying shrinkage strain would be a valuable input for numerical assessment of thermo-hydro-mechanical (THM) behaviour of structural concrete. Therefore, an approach that allows *a priori* estimation of drying shrinkage strain of hardened cement paste from the knowledge of cement composition and microstructural characteristics of the material paves a way forward for better understanding of the cracking potential of cementitious components or structures. Such an exercise is not limited to the aforementioned application alone but to other situations where drying shrinkage cracking is a problem, which underlines the necessity the importance and renovation of this framework.

The development of predictive models for drying shrinkage strain has significantly advanced in the last half a century (e.g. [6-10]). The basis for most of the advanced approaches rely on the idea of multiple mechanisms operating at different pore scales (Powers [11], Brochard et al. [12], Vandamme et al. [13], Pinson et al., [14] , Luan and Ishida [15], Nguyen et al. [16]) and importantly the approaches are relevant for reversible drying shrinkage strains only. The commonly adopted multiple mechanisms approach was in fact originally put forward by Powers [17], who presented a thermodynamic analysis of volumetric shrinkage strain of hardened cement paste attributable to solid surface tension or surface free energy (Eq. 12 in [11]), disjoining pressure (Eq. 17 [11]) and capillary pressure (Eq. 19 in [11]), but only included qualitative examples of individual volumetric strains. Their thermodynamic analysis essentially relates change in Gibb's free energy to water content in different pore classes via Kelvin's law and involves only one unknown constant in the disjoining pressure equation. A fundamental input is the water content in different pore classes: (de)sorption isotherm is the basis for this type of analysis and all similar approaches discussed further. Furthermore, they argue that the capillary pressure term represents the combined effect of both disjoining and capillary pressure for capillary pore range, but capillary pressure is not applicable for lower humidity range (~ <0.45), where only disjoining pressure is dominant. In what follows, particular attention is paid to the state of the art multi-mechanisms models for reversible drying shrinkage strain similar to that of Powers [11].

Coussy [9] showed that the capillary pressure alone cannot capture observed total volumetric strain of hardened cement paste and thus introduced an additional interfacial energy term, whose value increases with decrease in h. However, they conclude that their macroscopic approach of combining capillary pressure and interfacial energy fails to capture the macroscopic strain below relative humidity of 50-40%. Luan and Ishida [15] and Rezvani [18] used a multi-mechanism approach similar to Powers [11], in which they consider contribution of shrinkage

51 strains from capillary pressure and disjoining pressure only. In particular, Luan and Ishida [15]
52 argue that the effect of surface energy is only relevant at very low h and that the change in
53 disjoining pressure can be regarded as being equivalent to the change in surface energy at
54 complete desorption. They demonstrate excellent agreement with measured uniaxial shrinkage
55 strains for cement paste at two W/C ratios. Pinson et al.[14] also follow similar idea as Powers
56 [11] by proposing three mechanisms operating at three pore classes (capillary, gel and
57 interlayer) to capture total reversible shrinkage strain. Unlike Powers [11] who considers a
58 thermodynamic relationship for the shrinkage contribution due to disjoining pressure, Pinson
59 et al. [14] use a molecular approach plus a calibration factor to capture the shrinkage strain
60 contribution from the interlayer water. They also demonstrate a good agreement with desorption
61 experiment although their approach predicts a transitory swelling upon drying between about
62 30% and 20% RH. More recently, Nguyen et al. [16] proposed a multi-mechanism drying
63 shrinkage approach similar to Powers [11]. Starting from Gibb's free energy equation, they
64 derive a three-term equivalent pore pressure equation representing shrinkage contribution from
65 capillary pressure, surface free energy and disjoining pressure, which are then embedded within
66 a poroelastic theory to estimate the shrinkage strain. Note that their equivalent pore pressure is
67 not the same as Coussy [9], where only capillary and interfacial energy is considered. Two
68 calibration factors enter their drying shrinkage equation, one for the surface energy and the
69 other for disjoining pressure and it appears that they need to be calibrated for each material.
70 They show excellent correspondence with experimental results for Portland cement (CEM I)
71 cement for two different W/C ratios of 0.3 and 0.47. Finally, an interesting approach, which
72 does not belong to the afore mentioned multi-mechanism approaches, is that of Vlahinić et al.
73 [19] who proposes a constitutive model for drying of an elastic porous material based on the
74 Bishop [20] effective stress theory. In their approach, instead of pressure averaging, they
75 consider weakening of the solid as a function of drying (degree of saturation). They also show

an excellent agreement against a second cycle drying experiment on a 56-day-old cement paste sample. However, their model is valid under conditions where solid surface energy does not play an important role in deformation and where capillary pressure is dominant, in other words, h values above about 50% for hardened cement paste.

In conclusion, the validity of the multi-mechanism approach and the importance of sorption isotherm is sufficiently justified for drying shrinkage predictions. Keeping in mind the intended objective, which is to estimate drying shrinkage behaviour from cement composition, the study presented in this paper deviates from the aforementioned literatures in the following aspects:

i. A multiscale water (de)sorption isotherm framework (WSI) is invoked to estimate water content in different pore classes [21] (Section 2.1).
ii. An analytical homogenization approach principally based on Christensen [22, 23] is implemented to evaluate both the solid and bulk effective modulus of hardened cement paste (Section 2.2).
iii. A reversible drying shrinkage formulation is adopted comprising the Biot-Bishop's poroelasticity [20, 24], Bangham's relationship [14, 25] and Power's thermodynamic relationship [11] (Section 0).
iv. The role of microstructure on irreversible shrinkage strain is explored resulting in a phenomenological model that should be seen as a first approximation (Section 3.4.2).

The performance of the analytical framework is examined against a wide variety of drying shrinkage tests from literature, where complete data are available.

2 ANALYTICAL FRAMEWORK

An analytical framework for estimating drying shrinkage strain of hardened cement paste is implemented by combining existing approaches/models as follows (Figure 1):

i. An existing cement hydration kinetics model, Virtual Cement and Concrete Testing Laboratory (VCCTL), is used to estimate degree of hydration and volume fractions of Portlandite, C-S-H and capillary porosity based on the initial composition of the material. With the resultant degree of hydration, the volume fractions of high density (HD) and low density (LD) C-S-H is estimated via Jennings-Tennis's hydration model [26]. Depending on the ratio of HD and LD C-S-H, the porosity of the gel pore space is also derived ([21]). These volume fractions are used in estimating effective bulk modulus of the material (step (iii) below).

ii. A recently developed multiscale framework for estimating water desorption isotherm (WSI) [21] based on an integration of a number of models, which also includes step (i) above. This is the fundamental input necessary for computing drying shrinkage strain of the material for all the mechanisms considered.

iii. An existing analytical homogenization scheme is invoked to compute effective bulk modulus of the material based on inputs from (i) above. This parameter is an essential input for the unsaturated poromechanics theory to compute drying shrinkage strain due to capillary forces.

iv. An existing approach to estimate drying shrinkage strain principally based on the multi-mechanism approach proposed by Powers [11], which is based on thermodynamic equilibrium. The basic premise is that the total drying shrinkage strain can be attributed to a number of co-existing forces such as capillary, surface tension and disjoining pressure that operate at different relative humidity ranges, which are directly associated with the underlying pore size heterogeneity.

Of the above, only (iii) and (iv) are described in detail, whereas (i) and (ii) have already been dealt with in [21] but briefly covered in Section 2.1.

2.1 DESORPTION ISOTHERM FROM A MULTISCALE APPROACH

Babaei et al. [21] presented a multiscale framework to estimate desorption isotherm via the integration of the following models: (i) particle packing, (ii) cement hydration kinetics, and (iii) pore network. The first two models provide inputs for constructing pore size distribution as well as volume fractions of various pores, viz., gel (HD C-S-H, LD C-S-H) and capillary pores. The pore network model uses Kelvin's equation to determine distribution of equilibrium water content in the network for different increments of capillary pressure, P_c, in other words, the desorption isotherm for a given cement paste. For the shrinkage strain due to capillary forces, the desorption isotherm (i.e. P_c vs. S_w) provides direct input as required by Equation (7). For the shrinkage strain due to surface tension, the pore network model not only provides equilibrium volumetric water content (θ) as a function of P_c (or h), but also the volume of empty pores with surface adsorbed water, which is needed to compute σ as surface area of emptied pore per volume of porous material in Equation (10). For the disjoining pressure, the pore network model provides equilibrium water content (weight), w_d in pores smaller than 2.75 nm as a function of P_c (or h) (i.e. for $h < 0.45$) as required by Equation (12).

2.2 EFFECTIVE BULK MODULUS FROM ANALYTICAL HOMOGENIZATION

The effective bulk modulus of cement paste, K_b, is estimated using an analytical homogenization approach proposed by Christensen [22, 23] for two-phase material, which is based on Hashin's [27] composite spheres assemblage (CSA) model. The above can be generalized to a multiphase system as shown in Xi and Jennings [10]:

$$K_{s,eff} = K_{s,i} + \frac{s_{i-1,1}[(K_{s,eff})_{i-1} - K_{s,i}}{1 + (1 - s_{i-1,1})\dfrac{(K_{s,eff})_{i-1} - K_{s,i}}{K_{s,i} + {}^{4}/_{3}\, G_i}} \quad (1)$$

where $K_{s,i}$ and G_i are the bulk and shear modulus of different phases, respectively, and s is the volume fraction defined as:

$$s_{i-1,i} = \frac{\sum_{j=1}^{i-1} f_i}{\sum_{j=1}^{i} f_i} \qquad from\ i = 2\ to\ i = N-1 \quad (2)$$

$$s_{N-1,N} = 1 - f_N$$

f_i is the volume fraction of phase *i* such that:

$$\sum_{j=1}^{N} f_i = 1 \quad (3)$$

The homogenization sequence is illustrated in Figure 2. The first step computes effective bulk modulus of C-S-H gel by considering HD C-S-H and LD C-S-H as the two phases. The effect of gel pores in these phases are reflected in their stiffness values. The second step computes the effective bulk modulus of cement paste by considering a three-phase system: homogenized C-S-H gel obtained from the first step, Portlandite plus other crystalline hydration products, and the anhydrous cement grains.

The effective bulk modulus of solid skeleton is calculated using the abovementioned technique but to calculate the bulk modulus of porous structure, i.e. including capillary pores, Hashin and Shtrikman [28] found the effective bulk modulus for two-phase composite where voids are considered as a separate phase as follows:

$$K_b = K_{s,eff}\left(\frac{1 - \eta_c}{1 + \eta_c}\right) \quad (4)$$

Equation (4) was further modified as [29, 30]:

$$K_b = K_{s,eff}(1 - \eta_c)^2 \quad (5)$$

where η_c is the capillary porosity.

2.3 DRYING SHRINKAGE

Based on the proposal by Powers [11], the total shrinkage strain in pure OPC material may be attributed to three main mechanisms[11, 17, 31] :

i. ***Capillary forces***: Capillary water in pores are in a state of tension, which results in compressive stress in the solid phase, thus causing shrinkage of the material (Powers [31]). Powers [11] reasoned that capillary water cannot exist at h lower than approximately 0.45 because at this humidity only pores roughly above 2.6 nm will be de-saturated (or in equilibrium with h=0.45) on the basis of Kelvin-Laplace's equation. However, pores below 2.6 nm will be under the influence of strong interfacial forces (see point (iii) below) such that capillary menisci cannot be formed. Hence, the capillary-condensation theory is not valid anymore to estimate the drying shrinkage strain due to capillary forces. Therefore, shrinkage strain due to capillary forces (ε_{vc}) is postulated to operate in the relative humidity range 0.45 to 1.

ii. ***Solid surface tension***: Adsorption or desorption of water molecules on the surface of hardened cement microstructure is accompanied by a change in surface tension or equivalently surface free energy of the material. More specifically, there will be a decrease in energy during adsorption and an increase in energy during desorption. It is well documented that this change of energy is accompanied by volumetric strain (e.g. [32-34]). It is possible to relate the change in surface free energy to the change in vapour pressure by means of Gibb's equation ([25], [11] and [32]) and thus to the volumetric strain. Shrinkage strain due to solid surface tension (ε_{vs}) is postulated to operate in the entire relative humidity range of 0 to 1. This assumption is reasonable because at any

given humidity there will always be pores that will have adsorbed layer of water in a given representative volume element. Note that both Feldman and Sereda [32] and Pinson et al. [14] also consider it to be operative in the entire relative humidity range. It is however unclear if Powers [11, 17] considered the contribution of surface tension to the drying shrinkage strain above h=0.45.

iii. ***Disjoining pressure***: In the specific case of overlapping interfacial regions such as a thin layer of adsorbed water between two solid surfaces, the difference in the hydrostatic pressure of the adsorbed water in the interlayer and contiguous bulk water from which the adsorbed water phase was formed is referred to as the disjoining pressure [35, 36], and it is a function of thickness of the interlayer, and RH and temperature of the surrounding environment. For the disjoining pressure to be non-zero, the distance between the two solid surfaces must be less than a certain threshold value. For the case of hardened cement paste, Powers [11] estimated this value to be around 2.6 nm. He also estimated the mean inter-particle distance for the gel pores to be roughly 1.3 nm, which implies that the disjoining pressure can be active in majority of the gel pore space. This also implies that in this pore space, van der Waals attractive forces dominate giving rise to compressive forces between opposite surfaces, which are counter balanced by the disjoining pressure and the compressive stress of the solid phase (Powers, 1968 [17]). Therefore, it is imperative that any loss of water in the pore space due to drying is likely to result in shrinkage of the material. In light of the reasoning in point (i) above, the volumetric shrinkage strain due to disjoining pressure (ε_{vd}) is postulated to operate in the relative humidity range 0 to 0.45.

In the absence of external load and generally observed small strain (Pinson et al. [14]), the total reversible volumetric drying shrinkage strain ($\varepsilon_{v,r}$) can be mathematically expressed as:

$$\varepsilon_{v,r} = \varepsilon_{vc} + \varepsilon_{vs} + \varepsilon_{vd} \quad (6)$$

205

206 **2.3.1 SHRINKAGE STRAIN DUE TO CAPILLARY FORCES (0.45<h<1)**

207 Assuming pore air pressure (u_a) to be significantly smaller than pore water pressure (u_w), ε_{vc}
208 can be derived from the Bishop's "single effective stress" constitutive equation [20, 37] :

$$\varepsilon_{vc} = \frac{\chi P_c \alpha_B}{K_b} \quad (7)$$

$$\alpha_B = (1 - \frac{K_b}{K_s}) \quad (8)$$

$$P_c = (u_a - u_w) = \frac{RT}{M v_w} \ln(h) \quad (9)$$

209 where χ is the Bishop's effective stress parameter taken as equal to the degree of water
210 saturation (S_w), α_B is the Biot's coefficient, P_c is the capillary pressure (Pa), K_b is the bulk
211 modulus of the skeleton (Pa) and K_s is the bulk modulus of the solid phase (C-S-H) (Pa), R is
212 the gas constant (J/mol/K), T is the temperature (K), M is the molar mass of water (g/mol), v_w
213 is the specific volume of water (m^3/kg).

214 Especially, within the geomechanical/geotechnical community there are numerous discussions
215 on χ as well as applicability of single effective stress approach, which is beyond the scope of
216 this paper. Readers are referred to reviews by Jennings and Burland [38] and Nuth and Laloui
217 [39] concerning the single effective stress approach for partially saturated soils and the
218 difficulties in measuring a unique value of χ, and Vlahinic et al. [19] concerning the derivation
219 and interpretation of χ from micro-poromechanics. Nevertheless, Eq. (7) has been successfully
220 applied by Di Bella et al. [40] and appears to be fairly accurate for second cycle (or reversible
221 part) of drying but only at h>0.5.

2.3.2 SHRINKAGE STRAIN DUE TO SOLID SURFACE TENSION (0<h<1)

This study is similar to Pinson's [14] approach, which is essentially the Bangham equation [25] that describes volumetric strain from change of surface tension (surface free energy), ε_{vs}:

$$\varepsilon_{vs} = \frac{\Delta(\sigma\gamma)}{K_b} \tag{10}$$

where σ is the surface area of emptied pores per volume of porous material, which unlike Pinson [14], is directly obtained from the pore network model (Section 2.1). γ is the surface free energy of solid that is equal to additional surface tension of pore wall to the adsorbed water [14, 34] layer and it is computed via:

$$\gamma = \gamma_0 - \frac{RT}{M}\int_{h_0}^{h} \theta \frac{dh}{h} \tag{11}$$

where γ_0 is the surface tension at h_0, θ is the volumetric water content of the surface adsorbed water. h=1 is considered as the reference state with the corresponding surface tension set equal to the surface tension of bulk water.

2.3.3 SHRINKAGE STRAIN DUE TO DISJOINING PRESSURE (0 <h<0.45)

Based on a thermodynamic analysis, Powers [11] proposed an expression for the volumetric strain due to the disjoining pressure (Eq. (12)):

$$\varepsilon_{vd} = \kappa\beta' \frac{RT}{Mv_w}\int_{h1}^{h2} \frac{w_d}{V_s} dln(h) \tag{12}$$

where v_w is the molar volume of water, β' is the coefficient of compressibility of the material under sustained stress, which is taken as the inverse of bulk modulus of cement paste, K_b (Pa), and k is a constant of proportionality, which is taken as unity as a first approximation and w_d is water content is pores smaller than 2.75 nm. V_s is the volume of the adsorbent (m^3) defined as:

$$V_s = V_p(1 - \eta_t) \quad (13)$$

where V_p is the volume of cement paste and η_t is the total porosity of the paste.

2.3.4 OTHER MODELS FOR DRYING SHRINKAGE STRAIN

This study is particularly focussed on estimating drying shrinkage strain based on multi-mechanism approach (Section 0 to 2.3.3). However, there are other approaches, in particular, the equivalent pore pressure approach of Coussy et al. [9] and effective bulk modulus approach of Vlahinic et al. [19] that captures these mechanisms in a single framework. These are briefly covered in Appendix-A as the performance of the multi-mechanism approach will be compared with these single framework approaches.

3 VALIDATION

The analytical framework is validated against a number of available experimental data that encompass total shrinkage strains with and without irreversible strains for various hardened cement pastes [41-44]. The available experimental shrinkage strain is usually the ultimate shrinkage strain, which is an asymptotic value of the hyperbolic shrinkage strain equation as defined, for example, in ACI-209. Recall from Section 2-iv that the shrinkage strain equations (Equations (7), (10) and (12)) are based on thermodynamic equilibrium, which implies that the calculated strains are equilibrium values for a given *RH*, and hence can be directly compared with the experimental ultimate shrinkage strain. The shrinkage data are available for two types of materials: (i) non-virgin samples that were dried and rewetted to yield total shrinkage strains without irreversible strain component (samples CP1 to CP3), and (ii) virgin samples that were cured (Table 1) right after casting and kept saturated to yield total shrinkage strains, which include irreversible strain component (samples CP4 to CP9). Desorption isotherms are also available for these materials [41]. Recall that the drying shrinkage formulation (Section 0) is only able to estimate reversible shrinkage strain, but not the total shrinkage strain that includes irreversible strain. Nevertheless, the main purpose of comparing the predicted results with the shrinkage experiments of virgin samples is to (ii) explore the extent of deviation between the predicted and measured values and (ii) to quantitatively evaluate the role of microstructure on the irreversibility. The chemical composition, curing condition and experimental techniques of the materials (CP1 to CP9) are presented in Table 1.

3.1 CEMENT HYDRATION KINETICS

The results obtained from the cement hydration kinetics model, VCCTL [45], are presented in Table 2, which includes degree of hydration, volume fractions of Portlandite, C-S-H, and capillary porosity at the end of the respective curing periods. Table 2 also includes the volume fractions of HD and LD C-S-H based on Jennings-Tennis's hydration model. Note that the

results for the samples CP1-CP3 were already reported in Babaei et al. [21], but reproduced here for immediate reference. As expected, the models predict higher volume fractions of LD C-S-H, capillary porosity and final degree of hydration for compositions with higher water to cement ratio, which are qualitatively consistent with the known behaviour of OPC [26, 46-48].

3.2 WATER DESORPTION ISOTHERMS

Based on the multiscale WSI framework of Babaei et al. [21], desorption isotherms for materials CP1 to CP9 are estimated. Figure 3 and Figure 4 shows a comparison of predicted and experimental results of desorption isotherms for CP1 to CP3 and CP4 to CP9, respectively. Once again note that the results for CP1-CP3 were already discussed in Babaei et al. [21], but reproduced here for immediate reference. For materials CP4 to CP9, it is seen that the predicted results show reasonably good correlation with experimental results. The coefficient of determination ranges from 0.88 to 0.95 for predicted isotherm desorption curves. This increases confidence in the use of the multiscale WSI framework. In other words, with the available knowledge of cement microstructure and the set of models used in the WSI framework, it is possible to arrive at the desorption isotherm directly from cement composition.

3.3 EFFECTIVE BULK MODULUS

Based on the volume fractions of various hydration products (Table 2) and experimental data on Young's modulus and Poisson's ratio of individual phases of the cement paste (Table 3), K_b and K_s of the materials CP1 to CP9 are estimated as shown in Table 4. With the exception of materials CP1, CP2 and CP8, the homogenization technique captures experimental K_b results well. The deviations in the case of CP1, CP2 and CP8 are attributable to the differences between the actual material and the microstructural model results, for instance, with respect to the volume fractions of various phases and ratio of LD and HD C-S-H.

3.4 DRYING SHRINKAGE STRAIN

3.4.1 NON-VIRGIN MATERIAL - REVERSIBLE STRAIN

Figure 5(a)-(c) show a comparison of ultimate drying shrinkage strain of non-virgin materials (CP1 to CP3) as a function of degree of saturation. Note that for CP3, the experimental drying range is above RH=0.45 (corresponding S_w=0.47), where the disjoining pressure is postulated to be inactive, hence the shrinkage strain attributable to the disjoining pressure is zero. Overall, the predicted values show good correspondence with experimental data with coefficient of determination of 0.98, 0.91 and 0.99 respectively for CP1, CP2 and CP3, although with a slight overestimation for CP1 and CP2 at very low degree of saturation. Even though the WRC for CP1 and CP3 are slightly less accurate, the drying shrinkage strains are reasonably well predicted. However, data concerning experimental uncertainty are not available to completely confirm the degree of accuracy. In relative terms, CP2 shows less overall accuracy based on the coefficient of determination (0.91). Note that CP2 has also the most unconventional composition i.e. w/c =0.8 and is a blended cement. The fundamental input for the construction of pore network originates from the cement hydration kinetics model, which provides volume fractions of various type of pores and hydration products; the latter also linked to the estimation of bulk modulus of the material. The accuracy of the microstructural model for such a blend relies on the extent of calibration (with isothermal calorimetric data) that have been performed with this unconventional material type, which could be one source of uncertainty. The consequence is that the predicted WRC is slightly less accurate in the entire range of degree of saturation. In addition, since CP2 has a lower strength compared to CP1 and CP3, there is a possibility that CP2 has higher microcrack density, which is not captured by the mutli-mechanism model.

Figure 5(a)-(c) also shows contributions from the three shrinkage mechanisms. The general trend is that the contribution of surface free energy to the shrinkage strain is relatively less than

the disjoining and capillary forces, but is still quantitatively important. The exception is however for CP2, where the contribution from surface free energy is more than the capillary forces. The exception is because the total porosity of CP2 is very high 0.47 (W/C=0.8), which is directly accounted for in the σ term in the surface free energy (Equation (10)). Whereas, for the capillary force, the porosity is reflected in two properties: (i) K_b (Equation (5)), and (ii) desorption isotherm. Firstly, although K_b is important, it does not explain the difference even if the predicted K_b is replaced with experimental K_b (Table 4). Secondly, the high porosity results in a desorption isotherm that is characterized by lower capillary pressure for a given degree of saturation, compared to the materials with lower W/C ratios (CP1 and CP3). This results in a lower contribution from the capillary forces to the total shrinkage strain. However, the validity of the assumption $\chi = S_w$ remains questionable.

Figure 6 presents a comparison of results from the analytical framework that includes multi-mechanisms, Coussy et al. [9] that includes interface energy (Appendix A1) and Vlahinic et al. [19] that includes effective bulk modulus (Appendix A2) for CP1-CP3. The coefficient of determination of the predicted results varies from 0.91 to 0.99, 0.21 to 0.97 and 0.49 to 0.79 for the analytical framework, Coussy et al. [9] and Vlahinic et al. [19] respectively, thus offering an improved confidence in the capability of the analytical framework. Recall that Coussy's model (Equation (16)) mainly relies on the WRC ($S_w P_c$) to capture interfacial energies, and is also stated to be reliable up to RH=0.4-0.5 according to Coussy et al. [9]. It is noted that as long as the capillary forces ($S_w P_c$) dominate (Figure 5a and 5c), Coussy's model shows reasonable correspondence with experimental data, which is the case with CP1 and CP3, although the deviation is much more with the latter. However, for CP2, which has a relatively high W/C=0.8, it is shown that the calculated surface forces (Equation (10)) and disjoining pressure (Equation (12)) are dominant compared to the capillary forces (Equation (7)) (Figure 5b). Therefore, Coussy's model shows considerable deviation, which implies that their interfacial energy term

348 does not fully compensate for the surface forces and disjoining pressure predicted by Equation
349 (10) and Equation (12), respectively, specifically for high W/C.

350 ### 3.4.2 VIRGIN MATERIAL - TOTAL STRAIN

351 Figure 7 (a)-(f) show a comparison of ultimate drying shrinkage strain of virgin materials (CP4
352 to CP9) as a function of degree of saturation. The predicted values generally show poor
353 correspondence with experimental data except in the higher saturation range (S_w>0.8). The
354 coefficient of determination for the multi-mechanism model ranges from 0.37 to 0.80 with a
355 mean value of 0.64, for Coussy's model it ranges from 0.27 to 0.70 with a mean value of 0.57
356 and for Vlahinic's model it ranges from 0.2 to 0.6 with a mean value of 0.36. This is to be
357 expected because during the first drying permanent deformation occurs (irreversible strain),
358 which accounts for 29% to 40% of the total ultimate shrinkage strain (Table 2). Irreversible
359 shrinkage may include processes such as densification of LD C-S-H [48-51] and/or formation
360 of microcracks [47, 51, 52] that are not captured by the multi-mechanism approach. In
361 particular, it is clear that the strain due to capillary forces, surface free energy and disjoining
362 pressure relies on two fundamental parameters, which are (i) desorption isotherm and (ii) bulk
363 modulus. Firstly, a constant bulk modulus is considered for all the mechanisms and hence no
364 microstructural changes are reflected. While it is possible to consider the variation of the bulk
365 modulus as a function of degree of saturation as in the effective bulk modulus concept
366 (Appendix A1) of Vlahinic et al. [19], it still cannot compensate for the difference between the
367 total strain and reversible strain, for example, as shown in Figure 7 (f) for CP9. Secondly,
368 desorption isotherm is not significantly sensitive to small microstructural changes (Section 3.1
369 in [21]) and thus even though desorption isotherm may be determined on virgin samples, it will
370 still not quantitatively reflect the microstructural changes.

371 To further explore the role of microstructure, irreversible shrinkage strains are extracted from
372 the experimental data for CP4-CP9 by subtracting the total shrinkage strain obtained from the

drying and wetting branch of the experimental isotherms at *RH=1*. Table 2 presents the maximum irreversible shrinkage strains for materials CP4-CP9 (column 11). A first observation is that the irreversible shrinkage strain is proportional to the extent of drying. For example, sample CP4 is subjected to more drying (S_w≈0.2) compared to CP7 (S_w≈0.35), and accordingly the irreversible shrinkage strain is slightly higher in the case of CP4. It is also seen that the higher the amount of LD C-S-H, the higher is the irreversibility (Figure 8(a) and Figure 8(b)). Jennings [46, 48] argued in his C-S-H conceptual model that drying densifies the low density C-S-H. Thus the experimental results confirm Jennings [46, 48] model. Furthermore, the only shrinking phase in the hardened cement matrix is C-S-H, therefore, it is evident that the volume fraction of C-S-H gel is proportional to the total shrinkage strain. Accordingly, Figure 8(c) shows the irreversible shrinkage strain as a function of product of volume fraction of LD C-S-H and total C-S-H. It is also observed that the surface area of the material has a noticeable influence on shrinkage [14, 32, 53]. Since surface energy is the only force active throughout the whole drying range (Figure 7), it can be a valid candidate for estimating irreversible component of shrinkage. Other factors affecting the irreversibility are the solid bulk modulus and porous bulk modulus, which are functions of volume fraction of various hydration products but mostly C-S-H and porosity. These factors provide a basis to propose a phenomenological approach to account for the volumetric irreversible shrinkage strain, $\varepsilon_{v,irr}$. One proposal could take the form:

$$\varepsilon_{v,irr} = (\varepsilon_{vs} V_{C-S-H} V_{LD\ C-S-H})/\eta_t \tag{14}$$

Where ε_{vs} is shrinkage due to surface free energy, V_{C-S-H} is volume fraction of C-S-H, $V_{LD\ C-S-H}$ is volume fraction of LD C-S-H. which is observed to be at least valid for the six datasets presented in this paper (Figure 8(d)). Adding $\varepsilon_{v,irr}$ with $\varepsilon_{v,r}$ will yield the total drying shrinkage strain as shown in Figure 7 (*legend: multi-mechanism*). It is seen that the multi-

396 mechanism model results now correspond well with the experimental data for virgin materials,
397 especially for CP6-CP9 with coefficient of determination of 0.99 for all the four. However, the
398 level of accuracy is less satisfactory for CP4 and CP5 whose coefficient of determination are
399 0.86 and 0.91, respectively indicating that the multi-mechanism approach may still be missing
400 some important mechanisms or it is possible that there are some experimental uncertainties. It
401 is important to note that Equation (14) is merely a phenomenological model, which happens to
402 work on these materials and no further conclusion can be made given such small number of
403 data points.

404

4 CONCLUSIONS

A new analytical framework to estimate drying shrinkage strain for OPC-based materials is presented. As a starting point, the framework principally requires cement composition, microstructural information and mechanical properties of hydrated phases. There are only two calibration parameters: (i) a geometric parameter used in the pore network model, and (ii) a constant in the disjoining pressure relationship, which is set to unity because of a lack of knowledge (hence strictly no calibration). Importantly, there is no need to calibrate these parameters for every experiment. The following specific conclusions are reached:

i. Predicted desorption isotherms are in good correspondence with wide ranging experimental data from literature. In this study, six isotherms have been validated, which is in addition to the eleven isotherms already validated by the authors in their previous work Babaei et al. [21, 54], thus offering further confidence in the pore network model that forms the core module of the multiscale WSI framework.

ii. With some exceptions, the predicted bulk modulus of hardened cement paste is in good agreement w.r.t. the experimental data from literature. The deviations are attributed to the uncertainty in the results of the hydration model.

iii. The chosen drying shrinkage formulation has offered reasonably good results and offers insights into the active mechanisms during drying. In particular, the general trend is that the contribution of surface free energy to the shrinkage strain is relatively less than the disjoining and capillary forces, but is still quantitatively important for accuracy. Moreover, this trend depends on the W/C ratio. The formulation performs generally well compared to the equivalent pore pressure and effective bulk modulus concepts.

iv. It is not surprising that the drying shrinkage formulation does not offer satisfactory results w.r.t. experiments on virgin materials, which are subject to first drying cycle.

Examining the experimental results vis-à-vis hydration kinetics model suggest that the higher the amount of LD C-S-H, the higher is the irreversibility. A phenomenological model is proposed that quantitatively captures the irreversible shrinkage strain.

ACKNOWLEDGEMENTS

The first author gratefully acknowledges PhD sponsorship offered by SCK CEN. The findings and conclusions in this paper are those of the authors and do not represent the official position of SCK CEN. Advice received from our colleague Dr. Tri Quoc Phung during microstructural modelling is gratefully acknowledged. We are also grateful to two anonymous reviewers of this paper for their constructive criticism, which improved the quality of this paper.

APPENDIX A

A1. EQUIVALENT PORE PRESSURE CONCEPT – COUSSY

Coussy et al. [9] used equivalent pore pressure concept to compute drying shrinkage strain. In their model, interface energy, U, was defined as the sum of energy of all the interfaces including, liquid-gas, solid-liquid and solid-gas:

$$U = \int_{S_w}^{1} P_c(s)ds \tag{15}$$

Equivalent pore pressure, π, is defined via:

$$\pi = P^* - U \tag{16}$$

where P^* is the average pore pressure ($S_w P_c$). The drying shrinkage strain is then calculated via:

$$\varepsilon = \frac{\alpha_B \pi}{K_b} \tag{17}$$

A2. EFFECTIVE BULK MODULUS CONCEPT – VLAHINIC ET AL.

Vlahinic et al. [19, 55] proposed a constitutive model, which considers loss of stiffness of the material as the main parameter that dictates the volumetric deformation, which is attributed to microstructural evolution during drying. Their approach deviates from Bishop [20], which considers average pore pressure as the main parameter that dictates the volumetric deformation. The loss of stiffness is thus expressed in the form of reduction of K_s with decrease in degree of saturation, $\overline{K}(S_w)$, which is an experimentally aided estimate as defined in Eq. (19).

$$\varepsilon_{vc} = P_c\left(\frac{1}{K_b} - \frac{1}{\overline{K}(S_w)}\right) \tag{18}$$

$$\overline{K}(S_w) \approx K_s - \frac{K_s - K_b}{\varphi_0}\varphi(S_w) \tag{19}$$

$$\varphi(S_w) = \frac{(1 - S_w)\varphi_0}{1 - S_w\varphi_0} \tag{20}$$

where φ is the porosity of the effective solid, φ_0 is the initial porosity and S_w is the degree of water saturation.

List of Tables

Table 1. Chemical composition of the samples (% mass).

Material code	Material	W/C	C3S	C2S	C3A	C4AF	Curing method	Experimental method	Extent of drying of samples (*RH*)	Reference
CP1*	CEM II	0.50	0.21	0.53	0.10	0.15	Endogenous curing conditions for 1 year	Drying controlled by saturated salt solutions, T=20°C	0.25	[43]
CP2*	CEM II	0.80	0.21	0.53	0.10	0.15	Endogenous curing conditions for 1 year	Drying controlled by saturated salt solutions, T=20°C	0.30	[43]
CP3*	CEM I	0.45	0.56	0.18	0.06	0.11	Immersion in limewater for 56 days then dried for 270 days and rewetted for 28 days	Drying progressively for 270 days using ASTM C157, T=25 ± 0.2	0.45	[44]
CP4	CEM I	0.55	0.62	0.19	0.07	0.10	Saturated conditions for 91 days (100% RH)	Climate chamber with *h* control using sodium hydrate solution. T=20°C	0.2	[41, 42]
CP5	CEM I	0.40	0.62	0.19	0.07	0.10	same	same	0.2	[41, 42]
CP6	CEM I	0.55	0.42	0.38	0.04	0.12	same	same	0.2	[41, 42]
CP7	CEM I	0.40	0.42	0.38	0.04	0.12	same	same	0.2	[41, 42]
CP8	CEM I	0.55	0.24	0.62	0.02	0.08	same	same	0.2	[41, 42]
CP9	CEM I	0.40	0.24	0.62	0.02	0.08	same	same	0.2	[41, 42]

* Babaei et al. [21]

Table 2. Results from the cement hydration kinetics model at the end of respective curing periods, including experimental data of shrinkage strains.

Material code	W/C	Volume fraction LD-CSH	Volume fraction HD-CSH	Total C-S-H	Capillary porosity	Total porosity	DOH	Portlandite	Unhydrated Clinker	Other products	Limestone	Experimental		
												Ultimate shrinkage (m^3/m^3)	Irreversible shrinkage (m^3/m^3)	Irreversible/ ultimate shrinkage
CP1*	0.50	0.28	0.10	0.38	0.21	0.31	0.85	0.11	0.06	0.04	0.10	-0.003721	-	-
CP2*	0.80	0.32	0.05	0.37	0.33	0.42	0.95	0.10	0.02	0.02	0.07	-0.005144	-	-
CP3*	0.45	0.27	0.23	0.50	0.17	0.28	0.82	0.12	0.06	0.05	-	-0.002960	-	-
CP4	0.55	0.39	0.09	0.48	0.21	0.32	0.88	0.12	0.04	0.04	-	-0.004906	-0.001709	0.40
CP5	0.40	0.25	0.27	0.52	0.14	0.25	0.78	0.12	0.08	0.03	-	-0.004106	-0.001219	0.35
CP6	0.55	0.41	0.10	0.51	0.21	0.34	0.88	0.09	0.04	0.02	-	-0.005210	-0.001804	0.36
CP7	0.40	0.25	0.27	0.52	0.15	0.27	0.78	0.10	0.08	0.03	-	-0.004255	-0.001189	0.29
CP8	0.55	0.39	0.10	0.49	0.20	0.33	0.88	0.08	0.07	0.03	-	-0.006282	-0.002673	0.40
CP9	0.40	0.23	0.28	0.51	0.14	0.28	0.78	0.09	0.09	0.03	-	-0.004366	-0.001312	0.29

* Babaei et al. [21]

Table 3. Mechanical properties of hardened cement paste constituents [56-59].

	E (GPa)	υ (-)
C-S-H Gel		
HD C-S-H	29.4±2.4	0.24
LD C-S-H	21.7±2.2	0.24
Cement Paste		
C_3S	135	0.3
C_2S	140	0.3
C_3A	145	0.3
C_4AF	125	0.3
CH	38	0.305
Other products	52	0.32

Table 4. Calculated bulk modulus vs experimental data.

Material code	Experimental bulk modulus (K_b) (GPa)	Calculated Bulk modulus (K_b) using proposed model (GPa)	Calculated solid bulk modulus (K_s) using proposed model
CP1	10.5	11.52	18.5
CP2	6.0	7.50	16.6
CP3	12	12.20	17.4
CP4	11.0	11.85	18.9
CP5	13.8	13.67	18.48
CP6	11.0	11.27	18.05
CP7	12.4	12.61	17.45
CP8	9.27	10.34	16.25
CP9	12.8	12.02	16.10

List of Figures

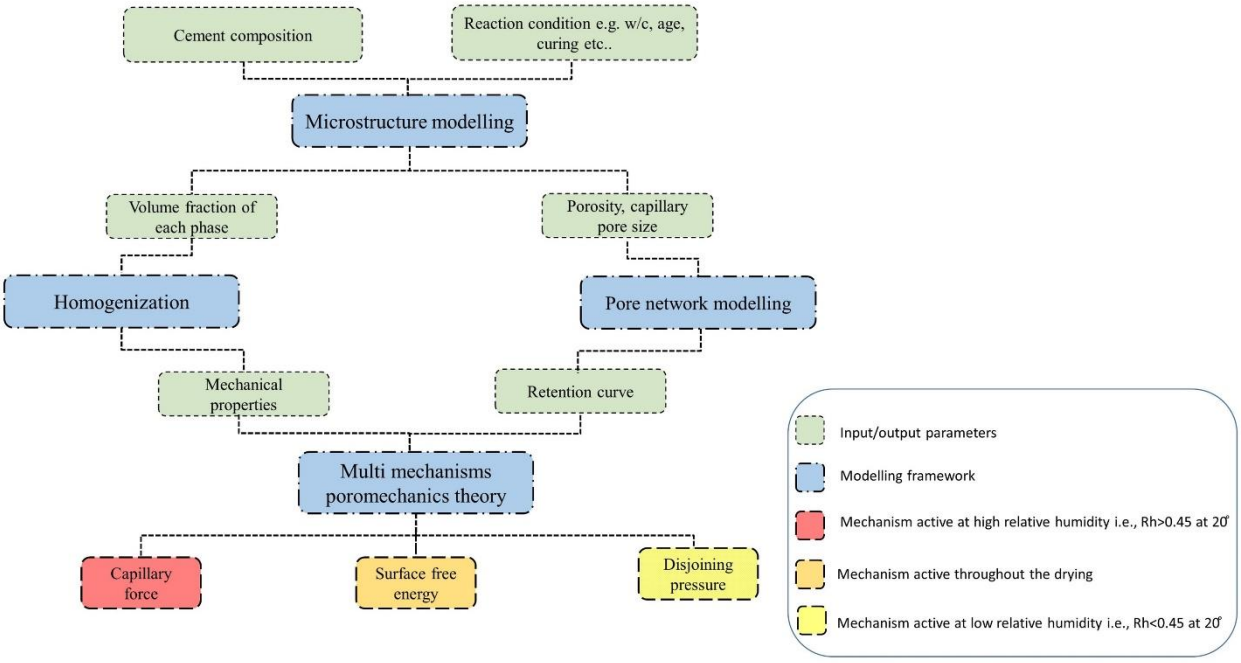

Figure 1. Analytical framework for estimating drying shrinkage strain.

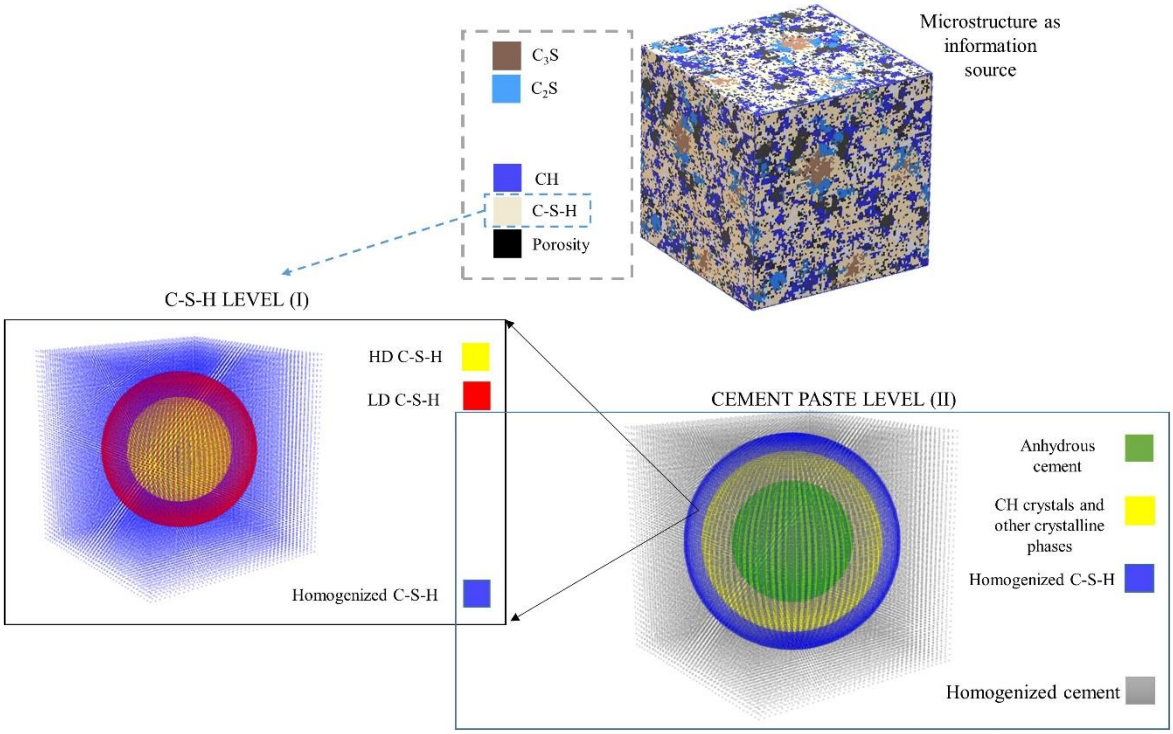

Figure 2. Generalized Homogenization method with its different levels.

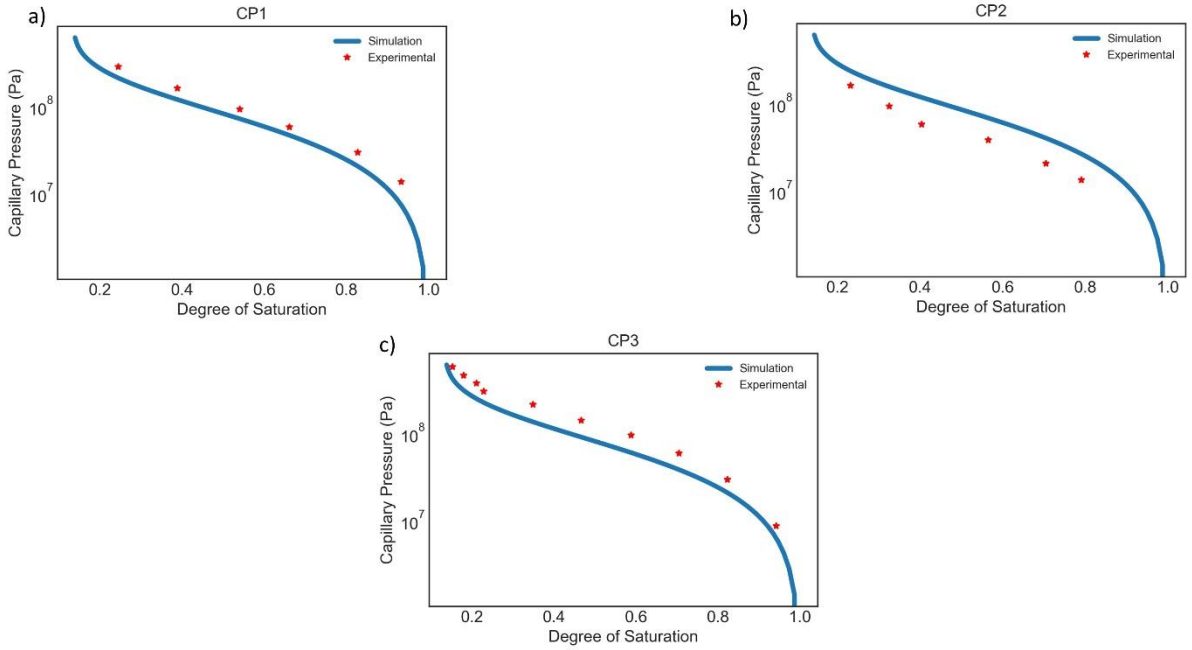

Figure 3. Estimated desorption isotherms for materials CP1-CP3 (previously reported in Babaei et al. [21].

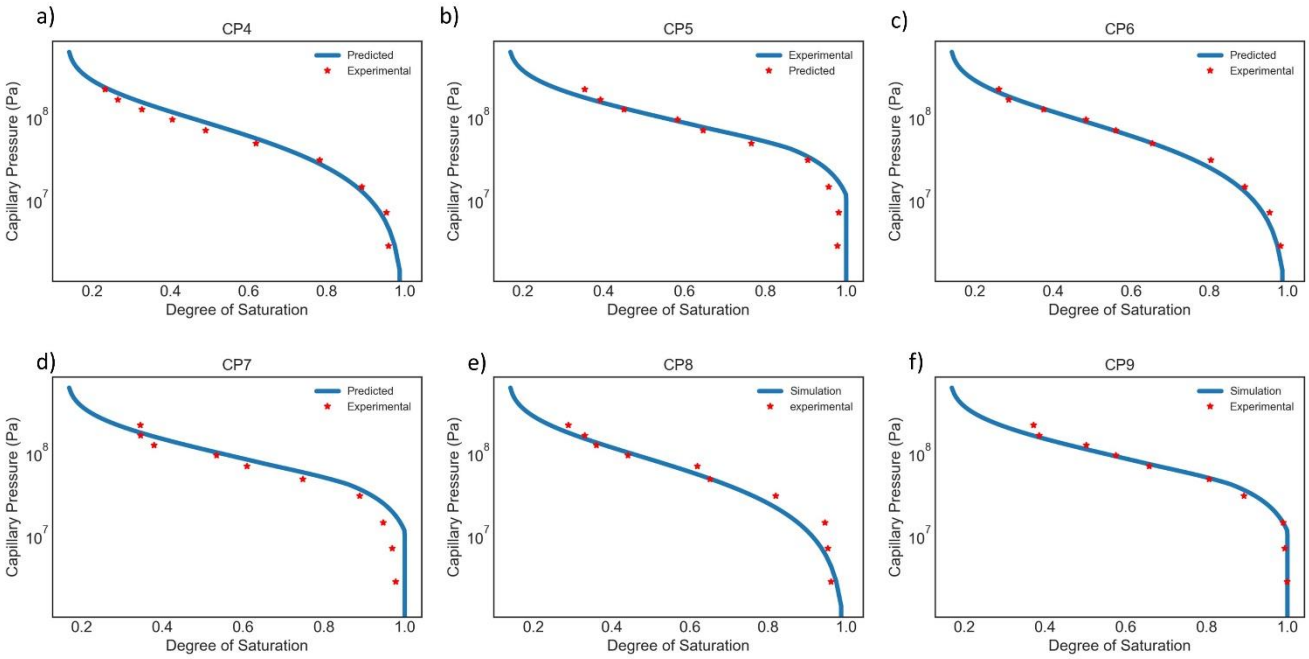

Figure 4. Estimated desorption isotherms for samples CP4-CP9 using Babaei et al. [21] approach vs experimental data.

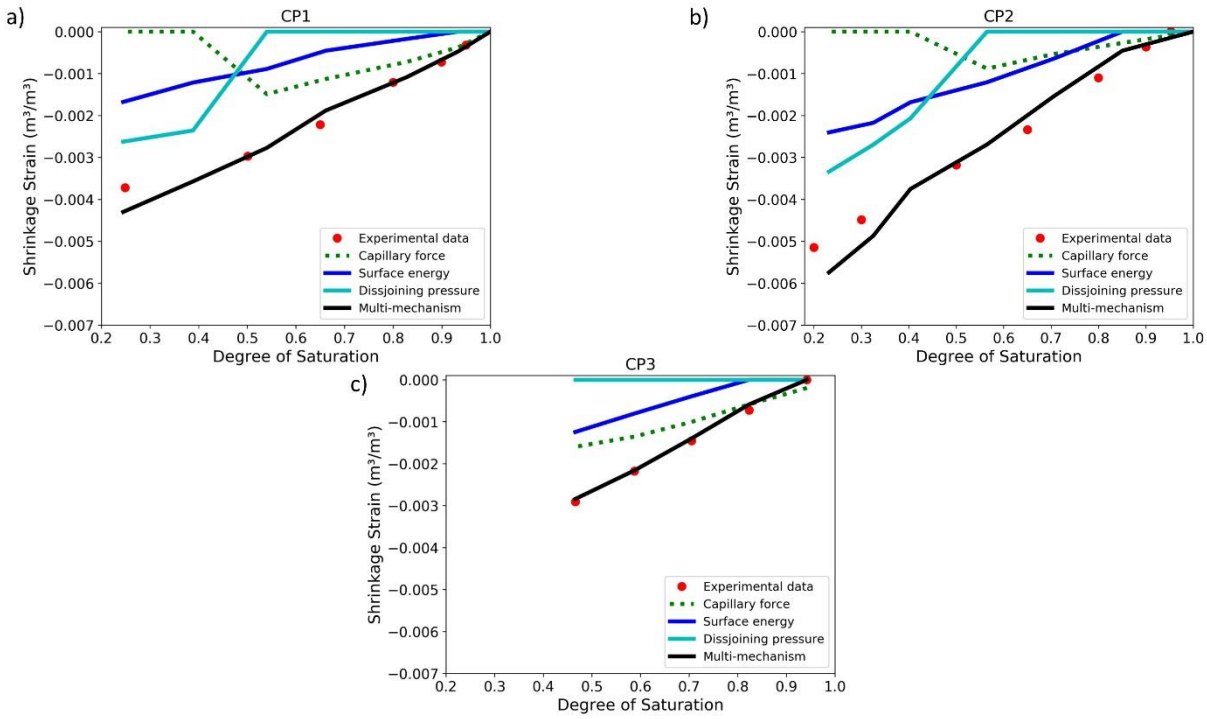

Figure 5. Contribution of each mechanism on predicted ultimate drying shrinkage vs. experimental data for non-virgin materials.

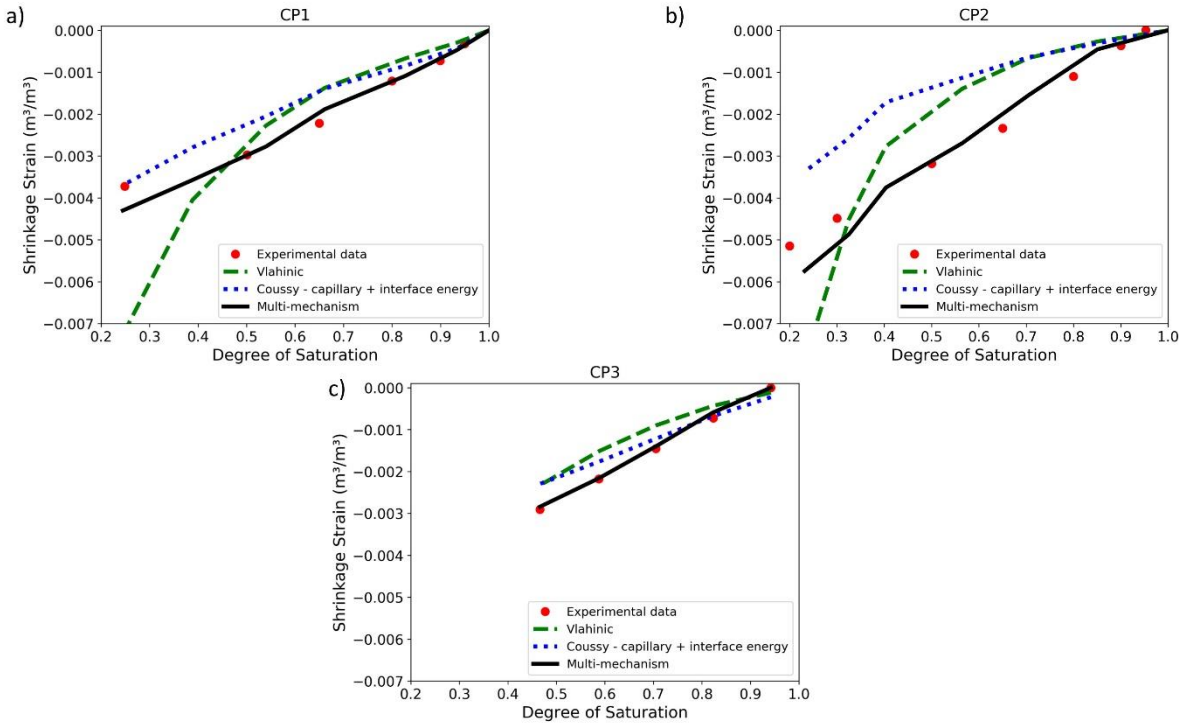

Figure 6. Predicted ultimate drying shrinkage from various models vs. experimental data for non-virgin materials.

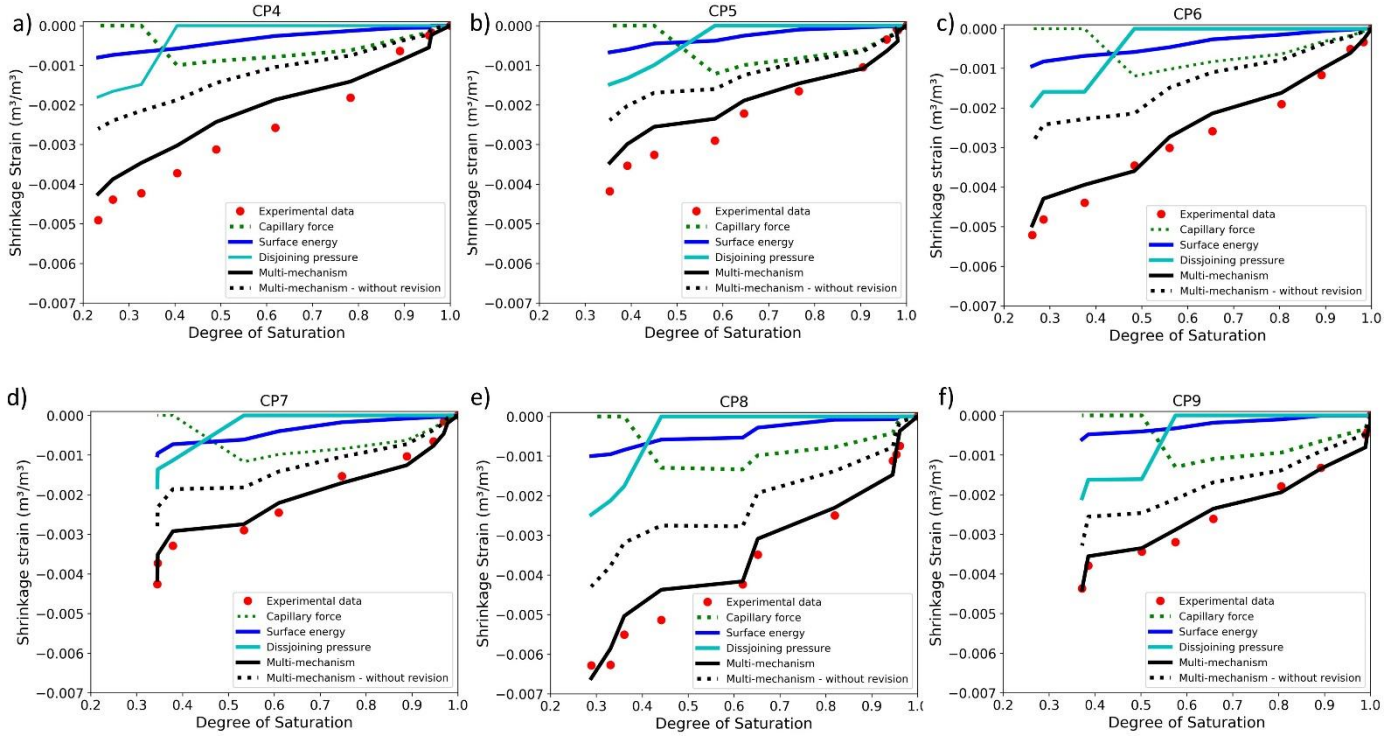

Figure 7. Contribution of each mechanism on predicted ultimate shrinkage vs experimental data for virgin materials. (multi-mechanism stands for proposed model plus experimental irreversible shrinkage)

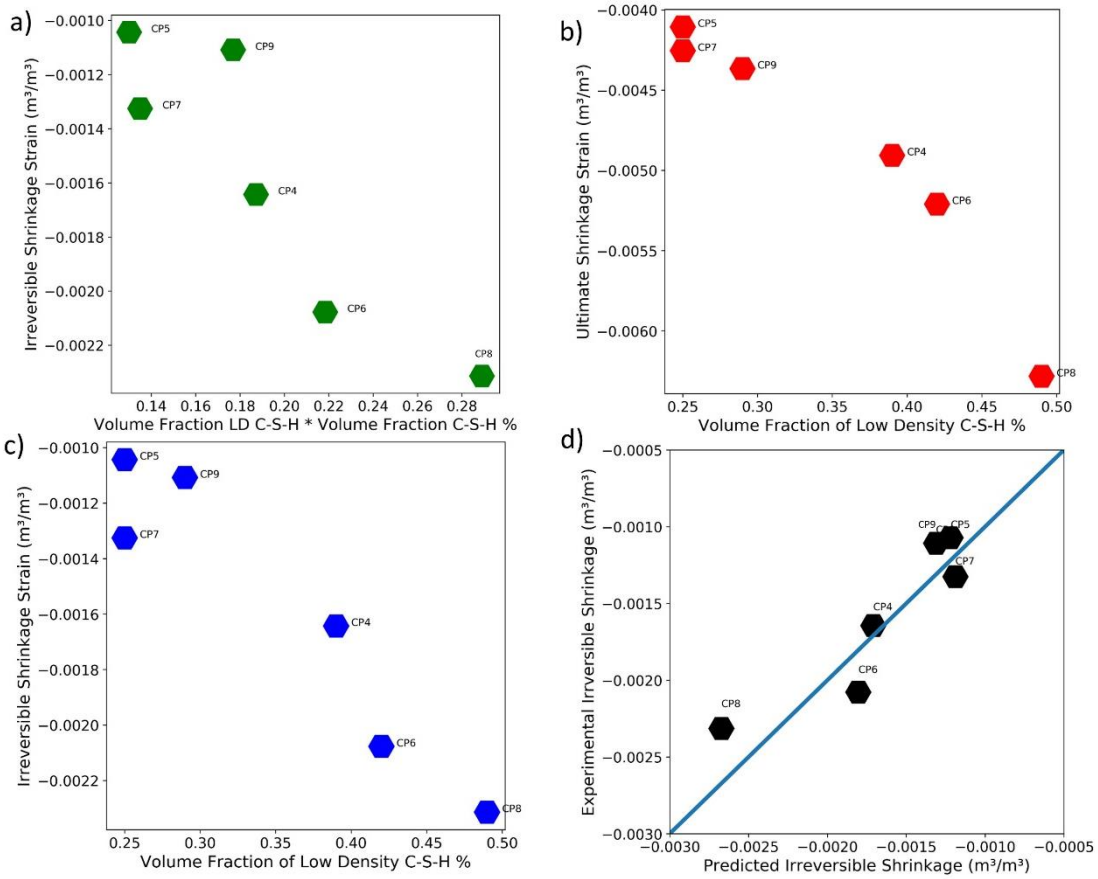

Figure 8. Irreversible shrinkage and its correlation with microstructural information.

1. Benboudjema, F., F. Meftah, and J.M. Torrenti, *A viscoelastic approach for the assessment of the drying shrinkage behaviour of cementitious materials.* Materials and Structures, 2006. **40**(2): p. 163.
2. Maruyama, I. and P. Lura, *Properties of early-age concrete relevant to cracking in massive concrete.* Cement and Concrete Research, 2019. **123**: p. 105770.
3. Craeye, B., et al., *Early age behaviour of concrete supercontainers for radioactive waste disposal.* Nuclear Engineering and Design, 2009. **239**(1): p. 23-35.
4. Craeye, B., et al., *Closure of the concrete supercontainer in hot cell under thermal load.* Nuclear Engineering and Design, 2011. **241**(5): p. 1352-1359.
5. J., B. and Bernier F., *Temperature Criterion Related to Clay Based Backfill Materials in the Framework of a Geological Repository of Heat Producing Radioactive Waste (HLW).* Proc. ICEM'Ol, The 8th International conference on Environmental Management, Bruges, Sept.30 - Oct.4, 2001.
6. *ACI-209 (2008), Guide for modeling and calculating shrinkage and creep in hardened concrete.* Farmington Hills, American Concrete Institute: p. 48.
7. *EN-1992-1-1 2008, Eurocode 2—design of concrete structures. Comite Europeen de Normalisation (CEN).* Brussels,: p. 259.
8. Bažant, Z.P. and S. Baweja, *Justification and refinements of model B3 for concrete creep and shrinkage 1. statistics and sensitivity.* Materials and Structures, 1995. **28**(7): p. 415-430.
9. Coussy, O., et al., *The equivalent pore pressure and the swelling and shrinkage of cement-based materials.* Materials and Structures, 2004. **37**(1): p. 15-20.
10. Xi, Y. and H.M. Jennings, *Shrinkage of cement paste and concrete modelled by a multiscale effective homogeneous theory.* Materials and Structures, 1997. **30**(6): p. 329.
11. Powers, T.C., *Mechanisms of Shrinkage and Reversible Creep of Hardened Cement Paste.* Conference Proceedings The Structure of Concrete, 1965.
12. Brochard, L., M. Vandamme, and R.J.M. Pellenq, *Poromechanics of microporous media.* Journal of the Mechanics and Physics of Solids, 2012. **60**(4): p. 606-622.
13. Vandamme, M., et al., *Modeling the Poromechanical Behavior of Microporousand Mesoporous Solids: Application to Coal*, in *Nonlinear Elasticity and Hysteresis*. 2014. p. 105-126.
14. Matthew B. Pinson, Enrico Masoero, and Hamlin M. Jennings, *Hysteresis from Multiscale Porosity: Modeling Water Sorption and Shrinkage in Cement Paste.* American Physical Society, 2015. **3**.
15. Luan, Y. and T. Ishida, *Enhanced Shrinkage Model Based on Early Age Hydration and Moisture Status in Pore Structure.* Journal of Advanced Concrete Technology, 2013. **11**(12): p. 360-373.
16. Nguyen, H., S. Rahimi-Aghdam, and Z.P. Bažant, *Unsaturated nanoporomechanics.* Proceedings of the National Academy of Sciences, 2020. **117**(7): p. 3440-3445.
17. POWERS, T.C., *The thermodynamics of volume change and creep.* Matériaux et Construction, 1968. **1**(6): p. 487–507.
18. Rezvani, M., T. Proske, and C.-A. Graubner, *Modelling the drying shrinkage of concrete made with limestone-rich cements.* Cement and Concrete Research, 2019. **115**: p. 160-175.
19. Vlahinić Ivan, Jennings Hamlin M., and Thomas Jeffrey J., *A constitutive model for drying of a partially saturated porous material.* Mechanics of Materials, 2009. **41**(3): p. 319-328.
20. Bishop, A.W., *The effective stress principle.* Teknisk Ukeblad 39, 1959: p. 859-863.
21. Babaei, S., et al., *A multiscale framework to estimate water sorption isotherms for OPC-based materials.* Cement and Concrete Composites, 2020. **105**: p. 103415.
22. Christensen, R.M., *Mechanics of Composite Materials.* Wiley-Interscience, New York,, 1979.
23. Christensen, R.M. and K.H. Lo, *Solutions for effective shear properties in three phase sphere and cylinder models.* Journal of the Mechanics and Physics of Solids, 1979. **27**(4): p. 315-330.
24. Biot, M.A., *Theory of Elasticity and Consolidation for a Porous Anisotropic Solid.* Journal of Applied Physics, 1955. **26**(2): p. 182-185.

25. Bangham, D.H. and R.I. Razouk, *The wetting of charcoal and the nature of the adsorbed phase formed from saturated vapours.* Transactions of the Faraday Society, 1937. **33**(0): p. 1463-1472.
26. Jennings H.M. and Tennis P.D., *A model for the developing microstructure in Portland cement pastes.* frAmer. Ceram. Soc, 1994. **77**(12): p. 3161-3172.
27. Hashin, Z., *Elastic moduli of heterogeneous materials.* Appl. Mech, 1962. **29**: p. 143–150.
28. Z. Hashin and S. Shtrikman, *A variational approach to the theory of the elastic behavior of multiphase materials.* J. Mech. Phys. Solids 1963. **11** p. 127–140.
29. W. Vichit-Vadakan and G.W. Scherer, *Measuring permeability of rigid materials by a beam-bending method: III. Cement paste.* Am. Ceram. Soc, 2002. **85**(6): p. 1537–44.
30. Z. Sun and G.W. Scherer, *Effect of air voids on salt scaling and internal freezing.* Cem. Concr. Res, 2010. **40**: p. 260–270.
31. Powers, T.C. and T.L. Brownyard, *Studies of the Physical Properties of Hardened Portland Cement Paste.* ACI Journal Proceedings. **43**(9).
32. Feldman, R.F. and P.J. SEREDA, *Sorption of water on compacts of bottle-hydrated cement. I. The sorption and length-change isotherms.* Journal of Applied Chemistry **14**(2): p. 87 - 93.
33. Feldman, R.F. and P.J. SEREDA, *SORPTION OF WATER ON COMPACTS OF BOTTLE-HYDRATED CEMENT. II* THERMODYNAMIC CONSIDERATIONS AND THEORY OF VOLUME CHANGE.* Journal of app Chem., February, 1964. **14**(2): p. 93-98.
34. HANSEN, W., *Drying Shrinkage Mechanisms in Portland Cement Paste.* Journal of the American Ceramic Society, 1987. **70**(5): p. 323-328.
35. Churaev, N.V., *The Relation between Colloid Stability and Wetting.* Journal of Colloid and Interface Science, 1995. **172**(2): p. 479-484.
36. Derjaguin, B.V., N.V. Churaev, and V.M. Muller, *Surface Forces.* Springer, Boston, MA, 1987.
37. Biot, M.A., *General Theory of Three-Dimensional Consolidation.* Journal of Applied Physics, 1941. **12**(2): p. 155-164.
38. Jennings, J.E.B. and J.B. Burland, *Limitations to the Use of Effective Stresses in Partly Saturated Soils.* Géotechnique, 1962. **12**(2): p. 125-144.
39. Nuth, M. and L. Laloui, *Effective stress concept in unsaturated soils: Clarification and validation of a unified framework.* International Journal for Numerical and Analytical Methods in Geomechanics, 2008. **32**(7): p. 771-801.
40. Mateusz Wyrzykowski, C.D.B., Pietro Lura, *Prediction of Drying Shrinkage of Cement-Based Mortars with Poroelastic Approaches - A Critical Review* Sixth Biot Conference on Poromechanics, Paris, France 2017. **6**: p. 579-586.
41. Maruyama, I., *Origin of Drying Shrinkage of Hardened Cement Paste: Hydration Pressure.* Journal of Advanced Concrete Technology 2010. **Vol. 8**(2): p. 187-200.
42. Ippei Maruyama, et al., *Microstructural and bulk property changes in hardened cement paste during the first drying process.* Cement and Concrete Research, 2014. **58**: p. 20–34.
43. Thomas Rougelot, Frédéric Skoczylas, and Nicolas Burlion, *Water desorption and shrinkage in mortars and cement pastes: Experimental study and poromechanical model.* Cement and Concrete Research, 2009. **39**: p. 36–44.
44. Galen Egan, et al., *Re-examining the influence of the inclusion characteristics on the drying shrinkage of cementitious composites.* Construction and Building Materials, 2017. **146**: p. 713-722.
45. Bullard J.W., *VCCTL Version 9.5 User Guide.* NIST, 2014.
46. Thomas J.J. and Jennings H.M., *A colloidal interpretation of chemical aging of the C-S-H gel and its effects on the properties of cement paste.* Cem Concr Res, 2006. **36**: p. 30-38.
47. Jennings H.M., et al., *A multi-technique investigation of the nanoporosity of cement paste.* Cem Concr Res, 2007. **37**: p. 329-336

48. Jennings, H.M., *Refinements to colloid model of C-S-H in cement: CM-II.* Cement and Concrete Research, 2008. **38**: p. 275–289.
49. Jennings, H.M., *A model for the microstructure of calcium silicate hydrate in cement paste.* Cement and Concrete Research, 2000. **30**: p. 101-116.
50. Hamlin M. Jennings, Aditya Kumar, and GauravSant, *Quantitative discrimination of the nano-pore-structure of cement paste during drying: New insights from water sorption isotherms.* Cement and Concrete Research 2015. **76**: p. 27-36.
51. Ippei Maruyama, et al., *Microstructural and bulk property changes in hardened cement paste during the first drying process.* Cement and Concrete Research, 2014. **58**: p. 20-34.
52. Ippei Maruyama, et al., *Microstructural changes in white Portland cement paste under the first drying process evaluated by WAXS, SAXS, and USAXS.* Cement and Concrete Research, 2017. **91**: p. 24-32.
53. Pinson, M., *Inferring Pore Size and Network Structure from Sorption Hysteresis.* 2014.
54. Babaei, S., et al., *Modeling of drying shrinkage in concrete : a multiscale poromechanics approach*, in *Symposium on Concrete Modelling : CONMOD2018, 26-29 August, 2018, Delft, the Netherlands*. 2018, RILEM Publications. p. 165-169.
55. Vlahinić, I., et al., *A novel and general form of effective stress in a partially saturated porous material: The influence of microstructure.* Mechanics of Materials, 2011. **43**(1): p. 25-35.
56. P. Acker, *Micromechanical analysis of creep and shrinkage mechanisms.* Creep, Shrinkage and Durability Mechanics of Concrete and other quasi-brittle Materials, 2001: p. 15-25.
57. Constantinides, G. and F.J. Ulm, *The effect of two types of C-S-H on the elasticity of cement-based materials: Results from nanoindentation and micromechanical modeling.* Cement and Concrete Research, 2004. **34**(1): p. 67-80.
58. Georgios Constantinides, *Invariant Mechanical Properties of Calcium-Silicate-Hydrates (C-S-H) in Cement-Based Materials: Instrumented Nanoindentation and Microporomechanical Modeling.* MASSACHUSETTS INSTITUTE OF TECHNOLOGY, 2006.
59. Ulm F.J., Constantinides G., and Heukamp F.H., *Is concrete a poromechanics material? – A multiscale investigation of poroelastic properties.* Mater Struct, 2004. **37**: p. 43-58.

An Analytical Framework for Estimating Drying Shrinkage Strain of OPC Based Hardened Cement Paste

Saeid Babaei[*(1)a,b,c], Suresh C. Seetharam[(2)a], Arnaud Dizier[(3)c], Gunther Steenackers[(4)b,d] and Bart Craeye[(5)b,e]

[a] Engineered and Geosystems Analysis Unit, Institute for Environment, Health, and Safety, Belgian Nuclear Research Centre (SCK•CEN), Boeretang 200, B-2400 Mol, Belgium.

[b] Faculty of Applied Engineering, University of Antwerp, EMIB Research Group, Groenenborgerlaan 171 - 2020 Antwerpen , Belgium

[c] EIG, EURIDICE, Belgian Nuclear Research Centre (SCK•CEN), Boeretang 200, B-2400 Mol, Belgium

[d] Faculty of Applied Engineering, University of Antwerp | Op3Mech Research Group Groenenborgerlaan 171 - 2020 Antwerpen

[e] Odisse University College, Industrial Services & Technologies, DUBIT Research Unit, Belgium

(1)* Tel: +32 14 333118, saeid.babaei@uantwerpen.be; saeid.babaei@sckcen.be

(2) Tel: +32 14 333208, suresh.seetharam@sckcen.be

(3) Tel: +32 14 332998, arnaud.dizier@euridice.be

(4) Tel: +32 00 000000, gunther.steenackers@uantwerpen.be

(5) Tel: +32 00 000000, bart.craeye@uantwerpen.be

ABSTRACT

A new analytical framework that relies on minimal inputs and combines a number of existing techniques to estimate reversible drying shrinkage strain of OPC-based materials is presented. This includes a multiscale framework for estimating water (de)sorption isotherm (WSI), an analytical homogenization technique to estimate bulk modulus, and a multi-mechanism based drying shrinkage formulation. The minimal inputs needed are the cement composition, microstructural information and mechanical properties of hydrated phases of hardened cement paste. A pore network model that forms the core module of the multiscale WSI provides a quantitative basis for the drying shrinkage formulation. The unique feature of the framework is that only two calibration parameters are involved: (i) a geometric parameter used in the pore network model, and (ii) a constant in the disjoining pressure relationship, which is set to unity mainly due to a lack of knowledge. Importantly, there is no need to calibrate these parameters for every experiment. Results from the framework are compared against shrinkage data from literature that encompass both virgin materials (samples that have never been dried prior to the test) and non-virgin materials. A reasonably good correspondence has been achieved with respect to the non-virgin materials, whereas, the results for the virgin materials are examined mainly to gain qualitative understanding of the role of the microstructure on irreversible deformation and thus to propose a phenomenological model.

KEYWORDS

Hardened cement paste, Drying shrinkage, Poroelasticity, Disjoining pressure, Surface free energy, Multi-mechanism shrinkage, Homogenization, Multiscale

1 INTRODUCTION

For massive civil engineering concrete structures, the drying shrinkage strain is usually neglected because water exchange with the surrounding environment is very slow and mostly its effect such as cracking is limited to a thin outer layer of the structure [1]. Moreover, in massive structures, peak temperature due to heat of hydration remains only for a few days thus limiting any adverse effect on drying rate [2]. However, this may not necessarily be the case in applications related to massive non-reinforced concrete engineered barriers for deep geological disposal of radioactive waste [3, 4]. In particular, the so-called Supercontainer concept currently under consideration in Belgium, encapsulates within a concrete buffer, high-level radioactive waste (HLW) materials that release decay heat over hundreds of years. Depending on the type of waste, temperatures can reach 100 ºC at the interface between the HLW canisters and concrete buffet [5], with an increased tendency to initiate a severe drying front at the interface and further into outer layers of the buffer. Therefore, the knowledge of drying shrinkage strain in the entire relative humidity (h) range becomes necessary. This is in addition to the contribution from other eigenstrains such as thermal and creep strains. In such applications, optimum choice of cement formulation at the design phase is essential and hence *a priori* knowledge of drying shrinkage strain would be a valuable input for numerical assessment of thermo-hydro-mechanical (THM) behaviour of structural concrete. Therefore, an approach that allows *a priori* estimation of drying shrinkage strain of hardened cement paste from the knowledge of cement composition and microstructural characteristics of the material paves a way forward for better understanding of the cracking potential of cementitious components or structures. Such an exercise is not limited to the aforementioned application alone but to other situations where drying shrinkage cracking is a problem, which underlines the necessity the importance and renovation of this framework.

The development of predictive models for drying shrinkage strain has significantly advanced in the last half a century (e.g. [6-10]). The basis for most of the advanced approaches rely on the idea of multiple mechanisms operating at different pore scales (Powers [11], Brochard et al. [12], Vandamme et al. [13], Pinson et al., [14] , Luan and Ishida [15], Nguyen et al. [16]) and importantly the approaches are relevant for reversible drying shrinkage strains only. The commonly adopted multiple mechanisms approach was in fact originally put forward by Powers [17], who presented a thermodynamic analysis of volumetric shrinkage strain of hardened cement paste attributable to solid surface tension or surface free energy (Eq. 12 in [11]), disjoining pressure (Eq. 17 [11]) and capillary pressure (Eq. 19 in [11]), but only included qualitative examples of individual volumetric strains. Their thermodynamic analysis essentially relates change in Gibb's free energy to water content in different pore classes via Kelvin's law and involves only one unknown constant in the disjoining pressure equation. A fundamental input is the water content in different pore classes: (de)sorption isotherm is the basis for this type of analysis and all similar approaches discussed further. Furthermore, they argue that the capillary pressure term represents the combined effect of both disjoining and capillary pressure for capillary pore range, but capillary pressure is not applicable for lower humidity range (~ <0.45), where only disjoining pressure is dominant. In what follows, particular attention is paid to the state of the art multi-mechanisms models for reversible drying shrinkage strain similar to that of Powers [11].

Coussy [9] showed that the capillary pressure alone cannot capture observed total volumetric strain of hardened cement paste and thus introduced an additional interfacial energy term, whose value increases with decrease in h. However, they conclude that their macroscopic approach of combining capillary pressure and interfacial energy fails to capture the macroscopic strain below relative humidity of 50-40%. Luan and Ishida [15] and Rezvani [18] used a multi-mechanism approach similar to Powers [11], in which they consider contribution of shrinkage

51 strains from capillary pressure and disjoining pressure only. In particular, Luan and Ishida [15]
52 argue that the effect of surface energy is only relevant at very low h and that the change in
53 disjoining pressure can be regarded as being equivalent to the change in surface energy at
54 complete desorption. They demonstrate excellent agreement with measured uniaxial shrinkage
55 strains for cement paste at two W/C ratios. Pinson et al.[14] also follow similar idea as Powers
56 [11] by proposing three mechanisms operating at three pore classes (capillary, gel and
57 interlayer) to capture total reversible shrinkage strain. Unlike Powers [11] who considers a
58 thermodynamic relationship for the shrinkage contribution due to disjoining pressure, Pinson
59 et al. [14] use a molecular approach plus a calibration factor to capture the shrinkage strain
60 contribution from the interlayer water. They also demonstrate a good agreement with desorption
61 experiment although their approach predicts a transitory swelling upon drying between about
62 30% and 20% RH. More recently, Nguyen et al. [16] proposed a multi-mechanism drying
63 shrinkage approach similar to Powers [11]. Starting from Gibb's free energy equation, they
64 derive a three-term equivalent pore pressure equation representing shrinkage contribution from
65 capillary pressure, surface free energy and disjoining pressure, which are then embedded within
66 a poroelastic theory to estimate the shrinkage strain. Note that their equivalent pore pressure is
67 not the same as Coussy [9], where only capillary and interfacial energy is considered. Two
68 calibration factors enter their drying shrinkage equation, one for the surface energy and the
69 other for disjoining pressure and it appears that they need to be calibrated for each material.
70 They show excellent correspondence with experimental results for Portland cement (CEM I)
71 cement for two different W/C ratios of 0.3 and 0.47. Finally, an interesting approach, which
72 does not belong to the afore mentioned multi-mechanism approaches, is that of Vlahinić et al.
73 [19] who proposes a constitutive model for drying of an elastic porous material based on the
74 Bishop [20] effective stress theory. In their approach, instead of pressure averaging, they
75 consider weakening of the solid as a function of drying (degree of saturation). They also show

an excellent agreement against a second cycle drying experiment on a 56-day-old cement paste sample. However, their model is valid under conditions where solid surface energy does not play an important role in deformation and where capillary pressure is dominant, in other words, h values above about 50% for hardened cement paste.

In conclusion, the validity of the multi-mechanism approach and the importance of sorption isotherm is sufficiently justified for drying shrinkage predictions. Keeping in mind the intended objective, which is to estimate drying shrinkage behaviour from cement composition, the study presented in this paper deviates from the aforementioned literatures in the following aspects:

i. A multiscale water (de)sorption isotherm framework (WSI) is invoked to estimate water content in different pore classes [21] (Section 2.1).
ii. An analytical homogenization approach principally based on Christensen [22, 23] is implemented to evaluate both the solid and bulk effective modulus of hardened cement paste (Section 2.2).
iii. A reversible drying shrinkage formulation is adopted comprising the Biot-Bishop's poroelasticity [20, 24], Bangham's relationship [14, 25] and Power's thermodynamic relationship [11] (Section 0).
iv. The role of microstructure on irreversible shrinkage strain is explored resulting in a phenomenological model that should be seen as a first approximation (Section 3.4.2).

The performance of the analytical framework is examined against a wide variety of drying shrinkage tests from literature, where complete data are available.

2 ANALYTICAL FRAMEWORK

An analytical framework for estimating drying shrinkage strain of hardened cement paste is implemented by combining existing approaches/models as follows (Figure 1):

i. An existing cement hydration kinetics model, Virtual Cement and Concrete Testing Laboratory (VCCTL), is used to estimate degree of hydration and volume fractions of Portlandite, C-S-H and capillary porosity based on the initial composition of the material. With the resultant degree of hydration, the volume fractions of high density (HD) and low density (LD) C-S-H is estimated via Jennings-Tennis's hydration model [26]. Depending on the ratio of HD and LD C-S-H, the porosity of the gel pore space is also derived ([21]). These volume fractions are used in estimating effective bulk modulus of the material (step (iii) below).

ii. A recently developed multiscale framework for estimating water desorption isotherm (WSI) [21] based on an integration of a number of models, which also includes step (i) above. This is the fundamental input necessary for computing drying shrinkage strain of the material for all the mechanisms considered.

iii. An existing analytical homogenization scheme is invoked to compute effective bulk modulus of the material based on inputs from (i) above. This parameter is an essential input for the unsaturated poromechanics theory to compute drying shrinkage strain due to capillary forces.

iv. An existing approach to estimate drying shrinkage strain principally based on the multi-mechanism approach proposed by Powers [11], which is based on thermodynamic equilibrium. The basic premise is that the total drying shrinkage strain can be attributed to a number of co-existing forces such as capillary, surface tension and disjoining pressure that operate at different relative humidity ranges, which are directly associated with the underlying pore size heterogeneity.

Of the above, only (iii) and (iv) are described in detail, whereas (i) and (ii) have already been dealt with in [21] but briefly covered in Section 2.1.

2.1 DESORPTION ISOTHERM FROM A MULTISCALE APPROACH

Babaei et al. [21] presented a multiscale framework to estimate desorption isotherm via the integration of the following models: (i) particle packing, (ii) cement hydration kinetics, and (iii) pore network. The first two models provide inputs for constructing pore size distribution as well as volume fractions of various pores, viz., gel (HD C-S-H, LD C-S-H) and capillary pores. The pore network model uses Kelvin's equation to determine distribution of equilibrium water content in the network for different increments of capillary pressure, P_c, in other words, the desorption isotherm for a given cement paste. For the shrinkage strain due to capillary forces, the desorption isotherm (i.e. P_c vs. S_w) provides direct input as required by Equation (7). For the shrinkage strain due to surface tension, the pore network model not only provides equilibrium volumetric water content (θ) as a function of P_c (or h), but also the volume of empty pores with surface adsorbed water, which is needed to compute σ as surface area of emptied pore per volume of porous material in Equation (10). For the disjoining pressure, the pore network model provides equilibrium water content (weight), w_d in pores smaller than 2.75 nm as a function of P_c (or h) (i.e. for $h < 0.45$) as required by Equation (12).

2.2 EFFECTIVE BULK MODULUS FROM ANALYTICAL HOMOGENIZATION

The effective bulk modulus of cement paste, K_b, is estimated using an analytical homogenization approach proposed by Christensen [22, 23] for two-phase material, which is based on Hashin's [27] composite spheres assemblage (CSA) model. The above can be generalized to a multiphase system as shown in Xi and Jennings [10]:

$$K_{s,eff} = K_{s,i} + \frac{s_{i-1,1}[(K_{s,eff})_{i-1} - K_{s,i}}{1 + (1 - s_{i-1,1})\dfrac{(K_{s,eff})_{i-1} - K_{s,i}}{K_{s,i} + {}^{4}/_{3}\, G_i}} \quad (1)$$

where $K_{s,i}$ and G_i are the bulk and shear modulus of different phases, respectively, and s is the volume fraction defined as:

$$s_{i-1,i} = \frac{\sum_{j=1}^{i-1} f_i}{\sum_{j=1}^{i} f_i} \qquad from\ i = 2\ to\ i = N-1 \quad (2)$$

$$s_{N-1,N} = 1 - f_N$$

f_i is the volume fraction of phase *i* such that:

$$\sum_{j=1}^{N} f_i = 1 \quad (3)$$

The homogenization sequence is illustrated in Figure 2. The first step computes effective bulk modulus of C-S-H gel by considering HD C-S-H and LD C-S-H as the two phases. The effect of gel pores in these phases are reflected in their stiffness values. The second step computes the effective bulk modulus of cement paste by considering a three-phase system: homogenized C-S-H gel obtained from the first step, Portlandite plus other crystalline hydration products, and the anhydrous cement grains.

The effective bulk modulus of solid skeleton is calculated using the abovementioned technique but to calculate the bulk modulus of porous structure, i.e. including capillary pores, Hashin and Shtrikman [28] found the effective bulk modulus for two-phase composite where voids are considered as a separate phase as follows:

$$K_b = K_{s,eff}\left(\frac{1 - \eta_c}{1 + \eta_c}\right) \quad (4)$$

Equation (4) was further modified as [29, 30]:

$$K_b = K_{s,eff}(1-\eta_c)^2 \quad (5)$$

where η_c is the capillary porosity.

2.3 DRYING SHRINKAGE

Based on the proposal by Powers [11], the total shrinkage strain in pure OPC material may be attributed to three main mechanisms[11, 17, 31] :

i. ***Capillary forces***: Capillary water in pores are in a state of tension, which results in compressive stress in the solid phase, thus causing shrinkage of the material (Powers [31]). Powers [11] reasoned that capillary water cannot exist at h lower than approximately 0.45 because at this humidity only pores roughly above 2.6 nm will be de-saturated (or in equilibrium with h=0.45) on the basis of Kelvin-Laplace's equation. However, pores below 2.6 nm will be under the influence of strong interfacial forces (see point (iii) below) such that capillary menisci cannot be formed. Hence, the capillary-condensation theory is not valid anymore to estimate the drying shrinkage strain due to capillary forces. Therefore, shrinkage strain due to capillary forces (ε_{vc}) is postulated to operate in the relative humidity range 0.45 to 1.

ii. ***Solid surface tension***: Adsorption or desorption of water molecules on the surface of hardened cement microstructure is accompanied by a change in surface tension or equivalently surface free energy of the material. More specifically, there will be a decrease in energy during adsorption and an increase in energy during desorption. It is well documented that this change of energy is accompanied by volumetric strain (e.g. [32-34]). It is possible to relate the change in surface free energy to the change in vapour pressure by means of Gibb's equation ([25], [11] and [32]) and thus to the volumetric strain. Shrinkage strain due to solid surface tension (ε_{vs}) is postulated to operate in the entire relative humidity range of 0 to 1. This assumption is reasonable because at any

given humidity there will always be pores that will have adsorbed layer of water in a given representative volume element. Note that both Feldman and Sereda [32] and Pinson et al. [14] also consider it to be operative in the entire relative humidity range. It is however unclear if Powers [11, 17] considered the contribution of surface tension to the drying shrinkage strain above h=0.45.

iii. ***Disjoining pressure***: In the specific case of overlapping interfacial regions such as a thin layer of adsorbed water between two solid surfaces, the difference in the hydrostatic pressure of the adsorbed water in the interlayer and contiguous bulk water from which the adsorbed water phase was formed is referred to as the disjoining pressure [35, 36], and it is a function of thickness of the interlayer, and RH and temperature of the surrounding environment. For the disjoining pressure to be non-zero, the distance between the two solid surfaces must be less than a certain threshold value. For the case of hardened cement paste, Powers [11] estimated this value to be around 2.6 nm. He also estimated the mean inter-particle distance for the gel pores to be roughly 1.3 nm, which implies that the disjoining pressure can be active in majority of the gel pore space. This also implies that in this pore space, van der Waals attractive forces dominate giving rise to compressive forces between opposite surfaces, which are counter balanced by the disjoining pressure and the compressive stress of the solid phase (Powers, 1968 [17]). Therefore, it is imperative that any loss of water in the pore space due to drying is likely to result in shrinkage of the material. In light of the reasoning in point (i) above, the volumetric shrinkage strain due to disjoining pressure (ε_{vd}) is postulated to operate in the relative humidity range 0 to 0.45.

In the absence of external load and generally observed small strain (Pinson et al. [14]), the total reversible volumetric drying shrinkage strain ($\varepsilon_{v,r}$) can be mathematically expressed as:

$$\varepsilon_{v,r} = \varepsilon_{vc} + \varepsilon_{vs} + \varepsilon_{vd} \quad (6)$$

205

206 **2.3.1 SHRINKAGE STRAIN DUE TO CAPILLARY FORCES (0.45<h<1)**

207 Assuming pore air pressure (u_a) to be significantly smaller than pore water pressure (u_w), ε_{vc}
208 can be derived from the Bishop's "single effective stress" constitutive equation [20, 37] :

$$\varepsilon_{vc} = \frac{\chi P_c \alpha_B}{K_b} \quad (7)$$

$$\alpha_B = (1 - \frac{K_b}{K_s}) \quad (8)$$

$$P_c = (u_a - u_w) = \frac{RT}{M v_w} \ln(h) \quad (9)$$

209 where χ is the Bishop's effective stress parameter taken as equal to the degree of water
210 saturation (S_w), α_B is the Biot's coefficient, P_c is the capillary pressure (Pa), K_b is the bulk
211 modulus of the skeleton (Pa) and K_s is the bulk modulus of the solid phase (C-S-H) (Pa), R is
212 the gas constant (J/mol/K), T is the temperature (K), M is the molar mass of water (g/mol), v_w
213 is the specific volume of water (m^3/kg).

214 Especially, within the geomechanical/geotechnical community there are numerous discussions
215 on χ as well as applicability of single effective stress approach, which is beyond the scope of
216 this paper. Readers are referred to reviews by Jennings and Burland [38] and Nuth and Laloui
217 [39] concerning the single effective stress approach for partially saturated soils and the
218 difficulties in measuring a unique value of χ, and Vlahinic et al. [19] concerning the derivation
219 and interpretation of χ from micro-poromechanics. Nevertheless, Eq. (7) has been successfully
220 applied by Di Bella et al. [40] and appears to be fairly accurate for second cycle (or reversible
221 part) of drying but only at h>0.5.

2.3.2 SHRINKAGE STRAIN DUE TO SOLID SURFACE TENSION (0<h<1)

This study is similar to Pinson's [14] approach, which is essentially the Bangham equation [25] that describes volumetric strain from change of surface tension (surface free energy), ε_{vs}:

$$\varepsilon_{vs} = \frac{\Delta(\sigma\gamma)}{K_b} \tag{10}$$

where σ is the surface area of emptied pores per volume of porous material, which unlike Pinson [14], is directly obtained from the pore network model (Section 2.1). γ is the surface free energy of solid that is equal to additional surface tension of pore wall to the adsorbed water [14, 34] layer and it is computed via:

$$\gamma = \gamma_0 - \frac{RT}{M}\int_{h_0}^{h} \theta \frac{dh}{h} \tag{11}$$

where γ_0 is the surface tension at h_0, θ is the volumetric water content of the surface adsorbed water. h=1 is considered as the reference state with the corresponding surface tension set equal to the surface tension of bulk water.

2.3.3 SHRINKAGE STRAIN DUE TO DISJOINING PRESSURE (0 <h<0.45)

Based on a thermodynamic analysis, Powers [11] proposed an expression for the volumetric strain due to the disjoining pressure (Eq. (12)):

$$\varepsilon_{vd} = \kappa\beta' \frac{RT}{Mv_w}\int_{h1}^{h2} \frac{w_d}{V_s} dln(h) \tag{12}$$

where v_w is the molar volume of water, β' is the coefficient of compressibility of the material under sustained stress, which is taken as the inverse of bulk modulus of cement paste, K_b (Pa), and k is a constant of proportionality, which is taken as unity as a first approximation and w_d is water content is pores smaller than 2.75 nm. V_s is the volume of the adsorbent (m^3) defined as:

$$V_s = V_p(1 - \eta_t) \quad (13)$$

where V_p is the volume of cement paste and η_t is the total porosity of the paste.

2.3.4 OTHER MODELS FOR DRYING SHRINKAGE STRAIN

This study is particularly focussed on estimating drying shrinkage strain based on multi-mechanism approach (Section 0 to 2.3.3). However, there are other approaches, in particular, the equivalent pore pressure approach of Coussy et al. [9] and effective bulk modulus approach of Vlahinic et al. [19] that captures these mechanisms in a single framework. These are briefly covered in Appendix-A as the performance of the multi-mechanism approach will be compared with these single framework approaches.

3 VALIDATION

The analytical framework is validated against a number of available experimental data that encompass total shrinkage strains with and without irreversible strains for various hardened cement pastes [41-44]. The available experimental shrinkage strain is usually the ultimate shrinkage strain, which is an asymptotic value of the hyperbolic shrinkage strain equation as defined, for example, in ACI-209. Recall from Section 2-iv that the shrinkage strain equations (Equations (7), (10) and (12)) are based on thermodynamic equilibrium, which implies that the calculated strains are equilibrium values for a given *RH*, and hence can be directly compared with the experimental ultimate shrinkage strain. The shrinkage data are available for two types of materials: (i) non-virgin samples that were dried and rewetted to yield total shrinkage strains without irreversible strain component (samples CP1 to CP3), and (ii) virgin samples that were cured (Table 1) right after casting and kept saturated to yield total shrinkage strains, which include irreversible strain component (samples CP4 to CP9). Desorption isotherms are also available for these materials [41]. Recall that the drying shrinkage formulation (Section 0) is only able to estimate reversible shrinkage strain, but not the total shrinkage strain that includes irreversible strain. Nevertheless, the main purpose of comparing the predicted results with the shrinkage experiments of virgin samples is to (ii) explore the extent of deviation between the predicted and measured values and (ii) to quantitatively evaluate the role of microstructure on the irreversibility. The chemical composition, curing condition and experimental techniques of the materials (CP1 to CP9) are presented in Table 1.

3.1 CEMENT HYDRATION KINETICS

The results obtained from the cement hydration kinetics model, VCCTL [45], are presented in Table 2, which includes degree of hydration, volume fractions of Portlandite, C-S-H, and capillary porosity at the end of the respective curing periods. Table 2 also includes the volume fractions of HD and LD C-S-H based on Jennings-Tennis's hydration model. Note that the

275 results for the samples CP1-CP3 were already reported in Babaei et al. [21], but reproduced
276 here for immediate reference. As expected, the models predict higher volume fractions of LD
277 C-S-H, capillary porosity and final degree of hydration for compositions with higher water to
278 cement ratio, which are qualitatively consistent with the known behaviour of OPC [26, 46-48].

279 ## 3.2 WATER DESORPTION ISOTHERMS

280 Based on the multiscale WSI framework of Babaei et al. [21], desorption isotherms for materials
281 CP1 to CP9 are estimated. Figure 3 and Figure 4 shows a comparison of predicted and
282 experimental results of desorption isotherms for CP1 to CP3 and CP4 to CP9, respectively.
283 Once again note that the results for CP1-CP3 were already discussed in Babaei et al. [21], but
284 reproduced here for immediate reference. For materials CP4 to CP9, it is seen that the predicted
285 results show reasonably good correlation with experimental results. The coefficient of
286 determination ranges from 0.88 to 0.95 for predicted isotherm desorption curves. This increases
287 confidence in the use of the multiscale WSI framework. In other words, with the available
288 knowledge of cement microstructure and the set of models used in the WSI framework, it is
289 possible to arrive at the desorption isotherm directly from cement composition.

290 ## 3.3 EFFECTIVE BULK MODULUS

291 Based on the volume fractions of various hydration products (Table 2) and experimental data
292 on Young's modulus and Poisson's ratio of individual phases of the cement paste (Table 3), K_b
293 and K_s of the materials CP1 to CP9 are estimated as shown in Table 4. With the exception of
294 materials CP1, CP2 and CP8, the homogenization technique captures experimental K_b results
295 well. The deviations in the case of CP1, CP2 and CP8 are attributable to the differences between
296 the actual material and the microstructural model results, for instance, with respect to the
297 volume fractions of various phases and ratio of LD and HD C-S-H.

3.4 DRYING SHRINKAGE STRAIN

3.4.1 NON-VIRGIN MATERIAL - REVERSIBLE STRAIN

Figure 5(a)-(c) show a comparison of ultimate drying shrinkage strain of non-virgin materials (CP1 to CP3) as a function of degree of saturation. Note that for CP3, the experimental drying range is above RH=0.45 (corresponding S_w=0.47), where the disjoining pressure is postulated to be inactive, hence the shrinkage strain attributable to the disjoining pressure is zero. Overall, the predicted values show good correspondence with experimental data with coefficient of determination of 0.98, 0.91 and 0.99 respectively for CP1, CP2 and CP3, although with a slight overestimation for CP1 and CP2 at very low degree of saturation. Even though the WRC for CP1 and CP3 are slightly less accurate, the drying shrinkage strains are reasonably well predicted. However, data concerning experimental uncertainty are not available to completely confirm the degree of accuracy. In relative terms, CP2 shows less overall accuracy based on the coefficient of determination (0.91). Note that CP2 has also the most unconventional composition i.e. w/c =0.8 and is a blended cement. The fundamental input for the construction of pore network originates from the cement hydration kinetics model, which provides volume fractions of various type of pores and hydration products; the latter also linked to the estimation of bulk modulus of the material. The accuracy of the microstructural model for such a blend relies on the extent of calibration (with isothermal calorimetric data) that have been performed with this unconventional material type, which could be one source of uncertainty. The consequence is that the predicted WRC is slightly less accurate in the entire range of degree of saturation. In addition, since CP2 has a lower strength compared to CP1 and CP3, there is a possibility that CP2 has higher microcrack density, which is not captured by the mutli-mechanism model.

Figure 5(a)-(c) also shows contributions from the three shrinkage mechanisms. The general trend is that the contribution of surface free energy to the shrinkage strain is relatively less than

the disjoining and capillary forces, but is still quantitatively important. The exception is however for CP2, where the contribution from surface free energy is more than the capillary forces. The exception is because the total porosity of CP2 is very high 0.47 (W/C=0.8), which is directly accounted for in the σ term in the surface free energy (Equation (10)). Whereas, for the capillary force, the porosity is reflected in two properties: (i) K_b (Equation (5)), and (ii) desorption isotherm. Firstly, although K_b is important, it does not explain the difference even if the predicted K_b is replaced with experimental K_b (Table 4). Secondly, the high porosity results in a desorption isotherm that is characterized by lower capillary pressure for a given degree of saturation, compared to the materials with lower W/C ratios (CP1 and CP3). This results in a lower contribution from the capillary forces to the total shrinkage strain. However, the validity of the assumption $\chi = S_w$ remains questionable.

Figure 6 presents a comparison of results from the analytical framework that includes multi-mechanisms, Coussy et al. [9] that includes interface energy (Appendix A1) and Vlahinic et al. [19] that includes effective bulk modulus (Appendix A2) for CP1-CP3. The coefficient of determination of the predicted results varies from 0.91 to 0.99, 0.21 to 0.97 and 0.49 to 0.79 for the analytical framework, Coussy et al. [9] and Vlahinic et al. [19] respectively, thus offering an improved confidence in the capability of the analytical framework. Recall that Coussy's model (Equation (16)) mainly relies on the WRC ($S_w P_c$) to capture interfacial energies, and is also stated to be reliable up to RH=0.4-0.5 according to Coussy et al. [9]. It is noted that as long as the capillary forces ($S_w P_c$) dominate (Figure 5a and 5c), Coussy's model shows reasonable correspondence with experimental data, which is the case with CP1 and CP3, although the deviation is much more with the latter. However, for CP2, which has a relatively high W/C=0.8, it is shown that the calculated surface forces (Equation (10)) and disjoining pressure (Equation (12)) are dominant compared to the capillary forces (Equation (7)) (Figure 5b). Therefore, Coussy's model shows considerable deviation, which implies that their interfacial energy term

348 does not fully compensate for the surface forces and disjoining pressure predicted by Equation
349 (10) and Equation (12), respectively, specifically for high W/C.

350 ### 3.4.2 VIRGIN MATERIAL - TOTAL STRAIN

351 Figure 7 (a)-(f) show a comparison of ultimate drying shrinkage strain of virgin materials (CP4
352 to CP9) as a function of degree of saturation. The predicted values generally show poor
353 correspondence with experimental data except in the higher saturation range (S_w>0.8). The
354 coefficient of determination for the multi-mechanism model ranges from 0.37 to 0.80 with a
355 mean value of 0.64, for Coussy's model it ranges from 0.27 to 0.70 with a mean value of 0.57
356 and for Vlahinic's model it ranges from 0.2 to 0.6 with a mean value of 0.36. This is to be
357 expected because during the first drying permanent deformation occurs (irreversible strain),
358 which accounts for 29% to 40% of the total ultimate shrinkage strain (Table 2). Irreversible
359 shrinkage may include processes such as densification of LD C-S-H [48-51] and/or formation
360 of microcracks [47, 51, 52] that are not captured by the multi-mechanism approach. In
361 particular, it is clear that the strain due to capillary forces, surface free energy and disjoining
362 pressure relies on two fundamental parameters, which are (i) desorption isotherm and (ii) bulk
363 modulus. Firstly, a constant bulk modulus is considered for all the mechanisms and hence no
364 microstructural changes are reflected. While it is possible to consider the variation of the bulk
365 modulus as a function of degree of saturation as in the effective bulk modulus concept
366 (Appendix A1) of Vlahinic et al. [19], it still cannot compensate for the difference between the
367 total strain and reversible strain, for example, as shown in Figure 7 (f) for CP9. Secondly,
368 desorption isotherm is not significantly sensitive to small microstructural changes (Section 3.1
369 in [21]) and thus even though desorption isotherm may be determined on virgin samples, it will
370 still not quantitatively reflect the microstructural changes.

371 To further explore the role of microstructure, irreversible shrinkage strains are extracted from
372 the experimental data for CP4-CP9 by subtracting the total shrinkage strain obtained from the

373 drying and wetting branch of the experimental isotherms at *RH=1*. Table 2 presents the
374 maximum irreversible shrinkage strains for materials CP4-CP9 (column 11). A first observation
375 is that the irreversible shrinkage strain is proportional to the extent of drying. For example,
376 sample CP4 is subjected to more drying (S_w≈0.2) compared to CP7 (S_w≈0.35), and accordingly
377 the irreversible shrinkage strain is slightly higher in the case of CP4. It is also seen that the
378 higher the amount of LD C-S-H, the higher is the irreversibility (Figure 8(a) and Figure 8(b)).
379 Jennings [46, 48] argued in his C-S-H conceptual model that drying densifies the low density
380 C-S-H. Thus the experimental results confirm Jennings [46, 48] model. Furthermore, the only
381 shrinking phase in the hardened cement matrix is C-S-H, therefore, it is evident that the volume
382 fraction of C-S-H gel is proportional to the total shrinkage strain. Accordingly, Figure 8(c)
383 shows the irreversible shrinkage strain as a function of product of volume fraction of LD C-S-
384 H and total C-S-H. It is also observed that the surface area of the material has a noticeable
385 influence on shrinkage [14, 32, 53]. Since surface energy is the only force active throughout
386 the whole drying range (Figure 7), it can be a valid candidate for estimating irreversible
387 component of shrinkage. Other factors affecting the irreversibility are the solid bulk modulus
388 and porous bulk modulus, which are functions of volume fraction of various hydration products
389 but mostly C-S-H and porosity. These factors provide a basis to propose a phenomenological
390 approach to account for the volumetric irreversible shrinkage strain, $\varepsilon_{v,irr}$. One proposal could
391 take the form:

$$\varepsilon_{v,irr} = (\varepsilon_{vs} V_{C-S-H} V_{LD\ C-S-H})/\eta_t \quad (14)$$

392 Where ε_{vs} is shrinkage due to surface free energy, V_{C-S-H} is volume fraction of C-S-H,
393 $V_{LD\ C-S-H}$ is volume fraction of LD C-S-H. which is observed to be at least valid for the six
394 datasets presented in this paper (Figure 8(d)). Adding $\varepsilon_{v,irr}$ with $\varepsilon_{v,r}$ will yield the total drying
395 shrinkage strain as shown in Figure 7 (*legend: multi-mechanism*). It is seen that the multi-

396 mechanism model results now correspond well with the experimental data for virgin materials,
397 especially for CP6-CP9 with coefficient of determination of 0.99 for all the four. However, the
398 level of accuracy is less satisfactory for CP4 and CP5 whose coefficient of determination are
399 0.86 and 0.91, respectively indicating that the multi-mechanism approach may still be missing
400 some important mechanisms or it is possible that there are some experimental uncertainties. It
401 is important to note that Equation (14) is merely a phenomenological model, which happens to
402 work on these materials and no further conclusion can be made given such small number of
403 data points.

404

4 CONCLUSIONS

A new analytical framework to estimate drying shrinkage strain for OPC-based materials is presented. As a starting point, the framework principally requires cement composition, microstructural information and mechanical properties of hydrated phases. There are only two calibration parameters: (i) a geometric parameter used in the pore network model, and (ii) a constant in the disjoining pressure relationship, which is set to unity because of a lack of knowledge (hence strictly no calibration). Importantly, there is no need to calibrate these parameters for every experiment. The following specific conclusions are reached:

i. Predicted desorption isotherms are in good correspondence with wide ranging experimental data from literature. In this study, six isotherms have been validated, which is in addition to the eleven isotherms already validated by the authors in their previous work Babaei et al. [21, 54], thus offering further confidence in the pore network model that forms the core module of the multiscale WSI framework.

ii. With some exceptions, the predicted bulk modulus of hardened cement paste is in good agreement w.r.t. the experimental data from literature. The deviations are attributed to the uncertainty in the results of the hydration model.

iii. The chosen drying shrinkage formulation has offered reasonably good results and offers insights into the active mechanisms during drying. In particular, the general trend is that the contribution of surface free energy to the shrinkage strain is relatively less than the disjoining and capillary forces, but is still quantitatively important for accuracy. Moreover, this trend depends on the W/C ratio. The formulation performs generally well compared to the equivalent pore pressure and effective bulk modulus concepts.

iv. It is not surprising that the drying shrinkage formulation does not offer satisfactory results w.r.t. experiments on virgin materials, which are subject to first drying cycle.

Examining the experimental results vis-à-vis hydration kinetics model suggest that the higher the amount of LD C-S-H, the higher is the irreversibility. A phenomenological model is proposed that quantitatively captures the irreversible shrinkage strain.

ACKNOWLEDGEMENTS

The first author gratefully acknowledges PhD sponsorship offered by SCK CEN. The findings and conclusions in this paper are those of the authors and do not represent the official position of SCK CEN. Advice received from our colleague Dr. Tri Quoc Phung during microstructural modelling is gratefully acknowledged. We are also grateful to two anonymous reviewers of this paper for their constructive criticism, which improved the quality of this paper.

APPENDIX A

A1. EQUIVALENT PORE PRESSURE CONCEPT – COUSSY

Coussy et al. [9] used equivalent pore pressure concept to compute drying shrinkage strain. In their model, interface energy, U, was defined as the sum of energy of all the interfaces including, liquid-gas, solid-liquid and solid-gas:

$$U = \int_{S_w}^{1} P_c(s)ds \tag{15}$$

Equivalent pore pressure, π, is defined via:

$$\pi = P^* - U \tag{16}$$

where P^* is the average pore pressure ($S_w P_c$). The drying shrinkage strain is then calculated via:

$$\varepsilon = \frac{\alpha_B \pi}{K_b} \tag{17}$$

A2. EFFECTIVE BULK MODULUS CONCEPT – VLAHINIC ET AL.

Vlahinic et al. [19, 55] proposed a constitutive model, which considers loss of stiffness of the material as the main parameter that dictates the volumetric deformation, which is attributed to microstructural evolution during drying. Their approach deviates from Bishop [20], which considers average pore pressure as the main parameter that dictates the volumetric deformation. The loss of stiffness is thus expressed in the form of reduction of K_s with decrease in degree of saturation, $\overline{K}(S_w)$, which is an experimentally aided estimate as defined in Eq. (19).

$$\varepsilon_{vc} = P_c\left(\frac{1}{K_b} - \frac{1}{\overline{K}(S_w)}\right) \tag{18}$$

$$\overline{K}(S_w) \approx K_s - \frac{K_s - K_b}{\varphi_0}\varphi(S_w) \tag{19}$$

$$\varphi(S_w) = \frac{(1 - S_w)\varphi_0}{1 - S_w\varphi_0} \tag{20}$$

where φ is the porosity of the effective solid, φ_0 is the initial porosity and S_w is the degree of water saturation.

List of Tables

Table 1. Chemical composition of the samples (% mass).

Material code	Material	W/C	C3S	C2S	C3A	C4AF	Curing method	Experimental method	Extent of drying of samples (*RH*)	Reference
CP1*	CEM II	0.50	0.21	0.53	0.10	0.15	Endogenous curing conditions for 1 year	Drying controlled by saturated salt solutions, T=20°C	0.25	[43]
CP2*	CEM II	0.80	0.21	0.53	0.10	0.15	Endogenous curing conditions for 1 year	Drying controlled by saturated salt solutions, T=20°C	0.30	[43]
CP3*	CEM I	0.45	0.56	0.18	0.06	0.11	Immersion in limewater for 56 days then dried for 270 days and rewetted for 28 days	Drying progressively for 270 days using ASTM C157, T=25 ± 0.2	0.45	[44]
CP4	CEM I	0.55	0.62	0.19	0.07	0.10	Saturated conditions for 91 days (100% RH)	Climate chamber with h control using sodium hydrate solution. T=20°C	0.2	[41, 42]
CP5	CEM I	0.40	0.62	0.19	0.07	0.10	same	same	0.2	[41, 42]
CP6	CEM I	0.55	0.42	0.38	0.04	0.12	same	same	0.2	[41, 42]
CP7	CEM I	0.40	0.42	0.38	0.04	0.12	same	same	0.2	[41, 42]
CP8	CEM I	0.55	0.24	0.62	0.02	0.08	same	same	0.2	[41, 42]
CP9	CEM I	0.40	0.24	0.62	0.02	0.08	same	same	0.2	[41, 42]

* Babaei et al. [21]

Table 2. Results from the cement hydration kinetics model at the end of respective curing periods, including experimental data of shrinkage strains.

Material code	W/C	Volume fraction LD-CSH	Volume fraction HD-CSH	Total C-S-H	Capillary porosity	Total porosity	DOH	Portlandite	Unhydrated Clinker	Other products	Limestone	Experimental		
												Ultimate shrinkage (m^3/m^3)	Irreversible shrinkage (m^3/m^3)	Irreversible/ ultimate shrinkage
CP1*	0.50	0.28	0.10	0.38	0.21	0.31	0.85	0.11	0.06	0.04	0.10	-0.003721	-	-
CP2*	0.80	0.32	0.05	0.37	0.33	0.42	0.95	0.10	0.02	0.02	0.07	-0.005144	-	-
CP3*	0.45	0.27	0.23	0.50	0.17	0.28	0.82	0.12	0.06	0.05	-	-0.002960	-	-
CP4	0.55	0.39	0.09	0.48	0.21	0.32	0.88	0.12	0.04	0.04	-	-0.004906	-0.001709	0.40
CP5	0.40	0.25	0.27	0.52	0.14	0.25	0.78	0.12	0.08	0.03	-	-0.004106	-0.001219	0.35
CP6	0.55	0.41	0.10	0.51	0.21	0.34	0.88	0.09	0.04	0.02	-	-0.005210	-0.001804	0.36
CP7	0.40	0.25	0.27	0.52	0.15	0.27	0.78	0.10	0.08	0.03	-	-0.004255	-0.001189	0.29
CP8	0.55	0.39	0.10	0.49	0.20	0.33	0.88	0.08	0.07	0.03	-	-0.006282	-0.002673	0.40
CP9	0.40	0.23	0.28	0.51	0.14	0.28	0.78	0.09	0.09	0.03	-	-0.004366	-0.001312	0.29

* Babaei et al. [21]

Table 3. Mechanical properties of hardened cement paste constituents [56-59].

	E (GPa)	υ (-)
C-S-H Gel		
HD C-S-H	29.4±2.4	0.24
LD C-S-H	21.7±2.2	0.24
Cement Paste		
C_3S	135	0.3
C_2S	140	0.3
C_3A	145	0.3
C_4AF	125	0.3
CH	38	0.305
Other products	52	0.32

Table 4. Calculated bulk modulus vs experimental data.

Material code	Experimental bulk modulus (K_b) (GPa)	Calculated Bulk modulus (K_b) using proposed model (GPa)	Calculated solid bulk modulus (K_s) using proposed model
CP1	10.5	11.52	18.5
CP2	6.0	7.50	16.6
CP3	12	12.20	17.4
CP4	11.0	11.85	18.9
CP5	13.8	13.67	18.48
CP6	11.0	11.27	18.05
CP7	12.4	12.61	17.45
CP8	9.27	10.34	16.25
CP9	12.8	12.02	16.10

List of Figures

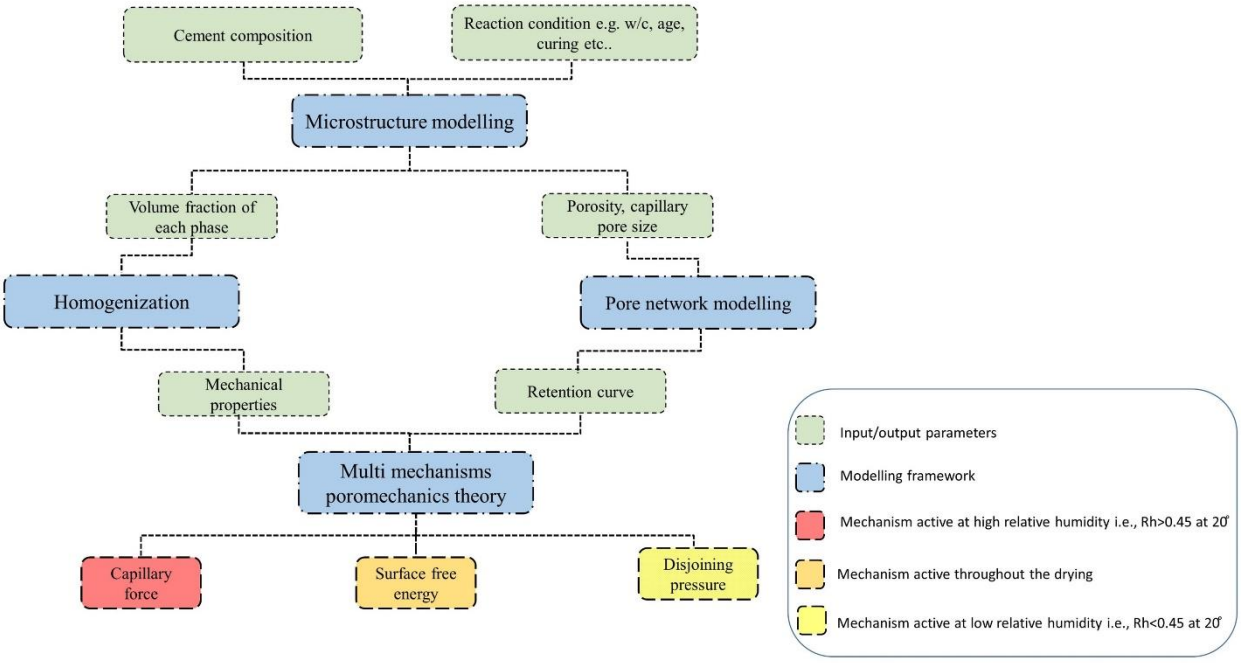

Figure 1. Analytical framework for estimating drying shrinkage strain.

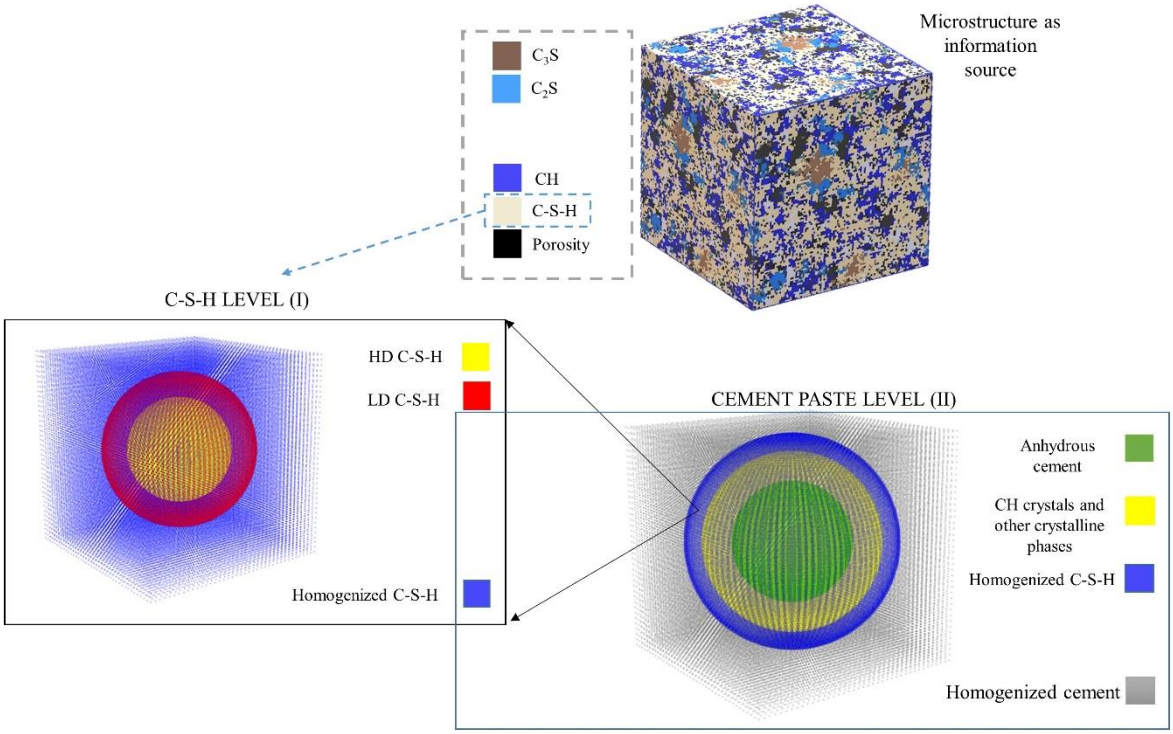

Figure 2. Generalized Homogenization method with its different levels.

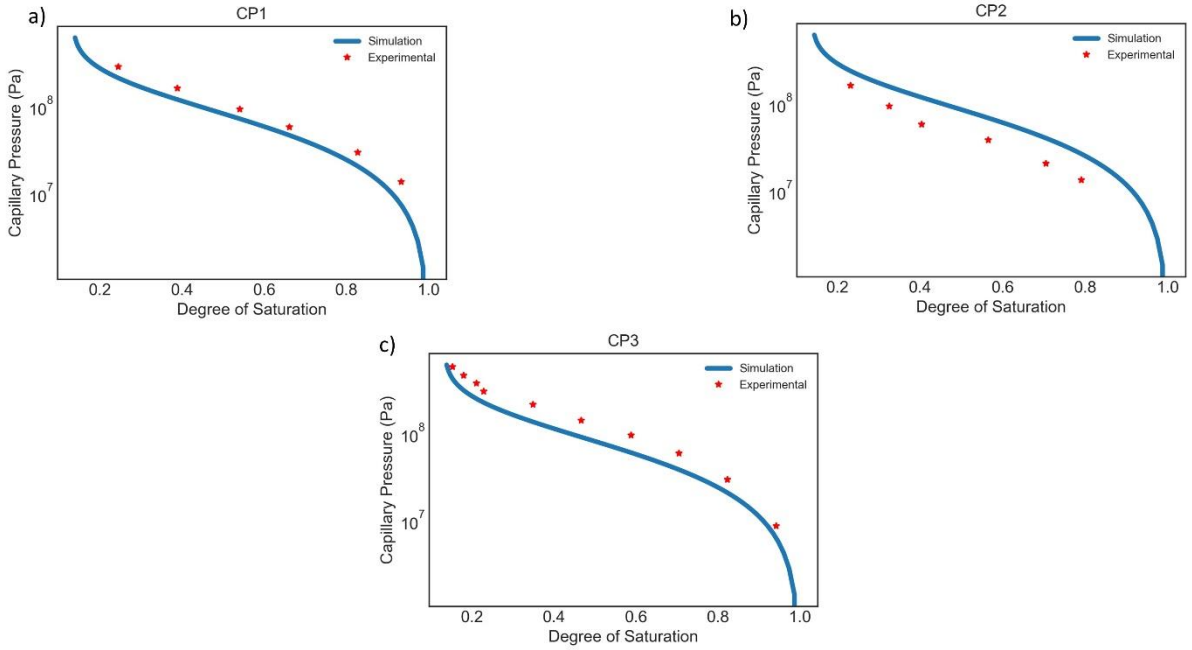

Figure 3. Estimated desorption isotherms for materials CP1-CP3 (previously reported in Babaei et al. [21].

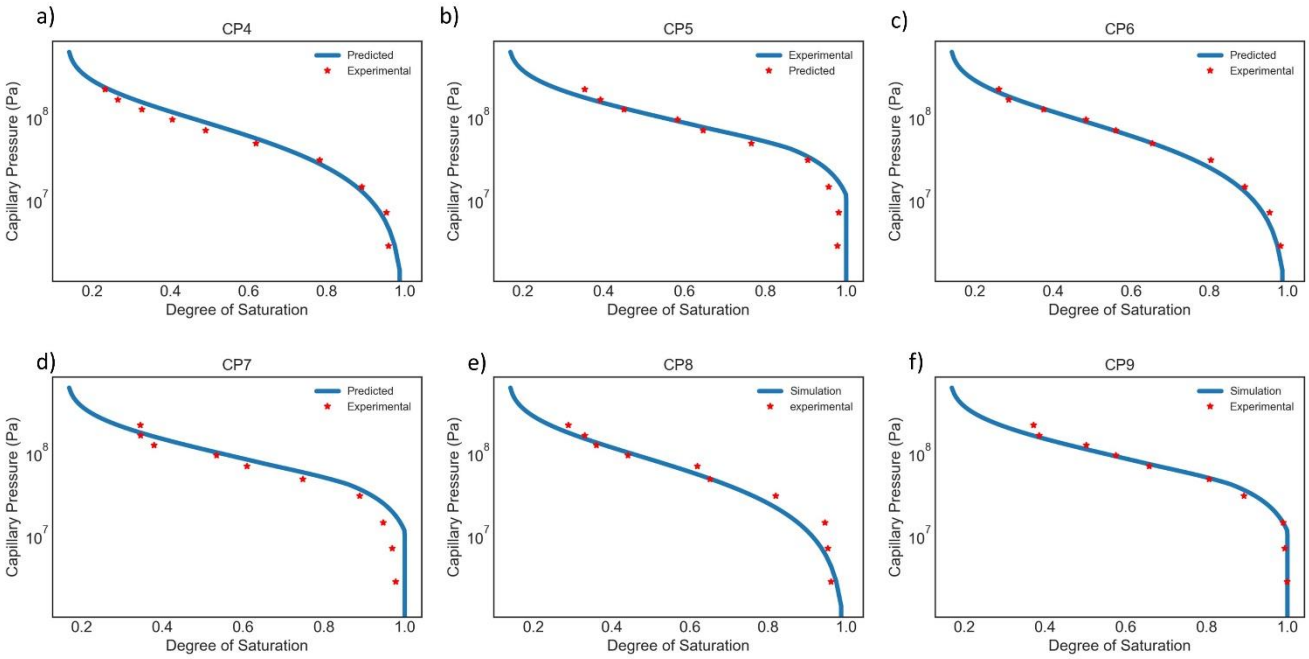

Figure 4. Estimated desorption isotherms for samples CP4-CP9 using Babaei et al. [21] approach vs experimental data.

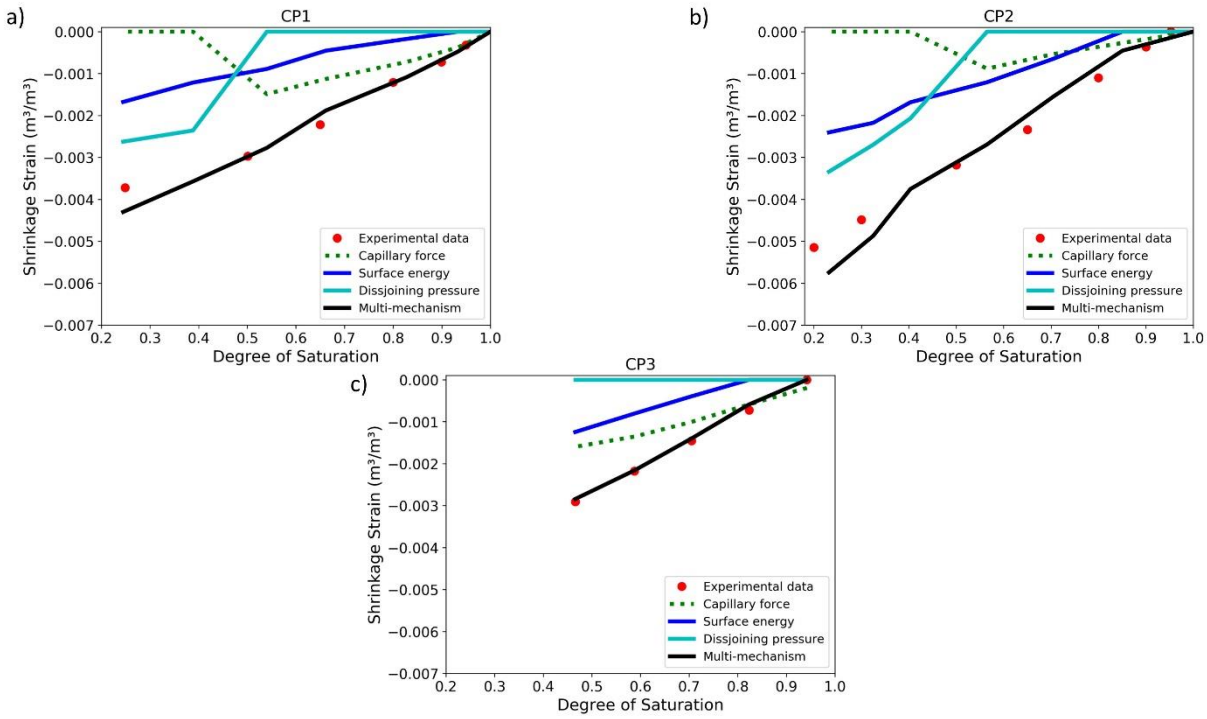

Figure 5. Contribution of each mechanism on predicted ultimate drying shrinkage vs. experimental data for non-virgin materials.

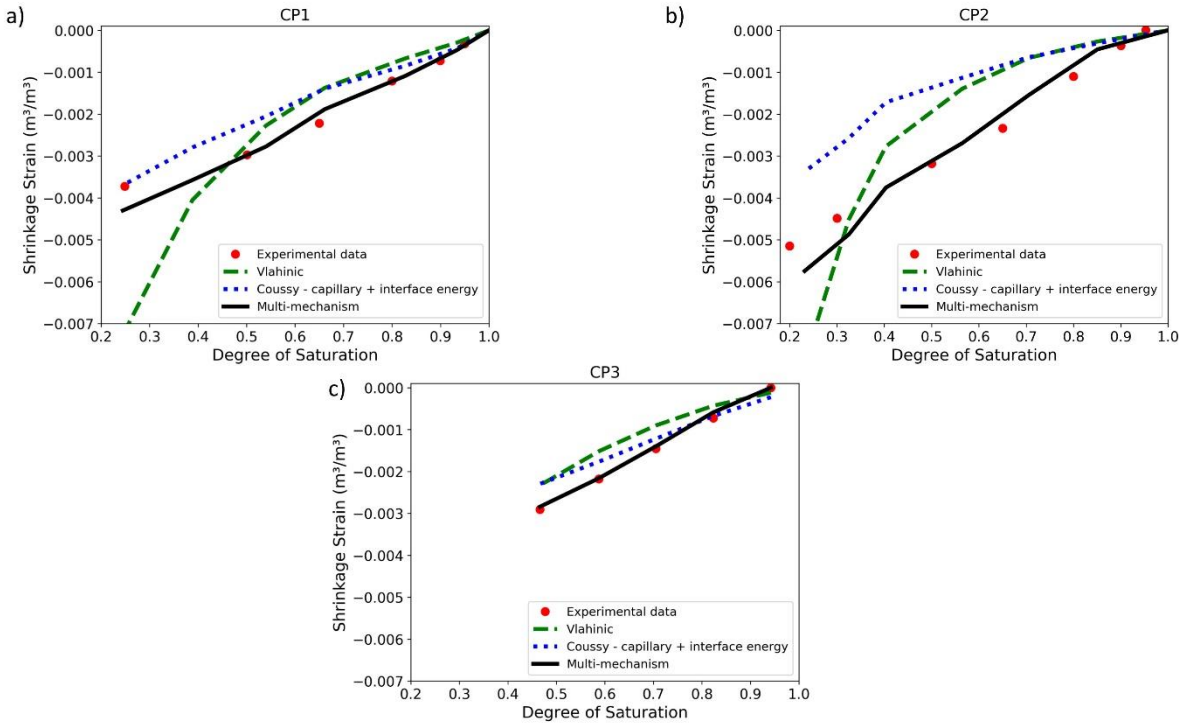

Figure 6. Predicted ultimate drying shrinkage from various models vs. experimental data for non-virgin materials.

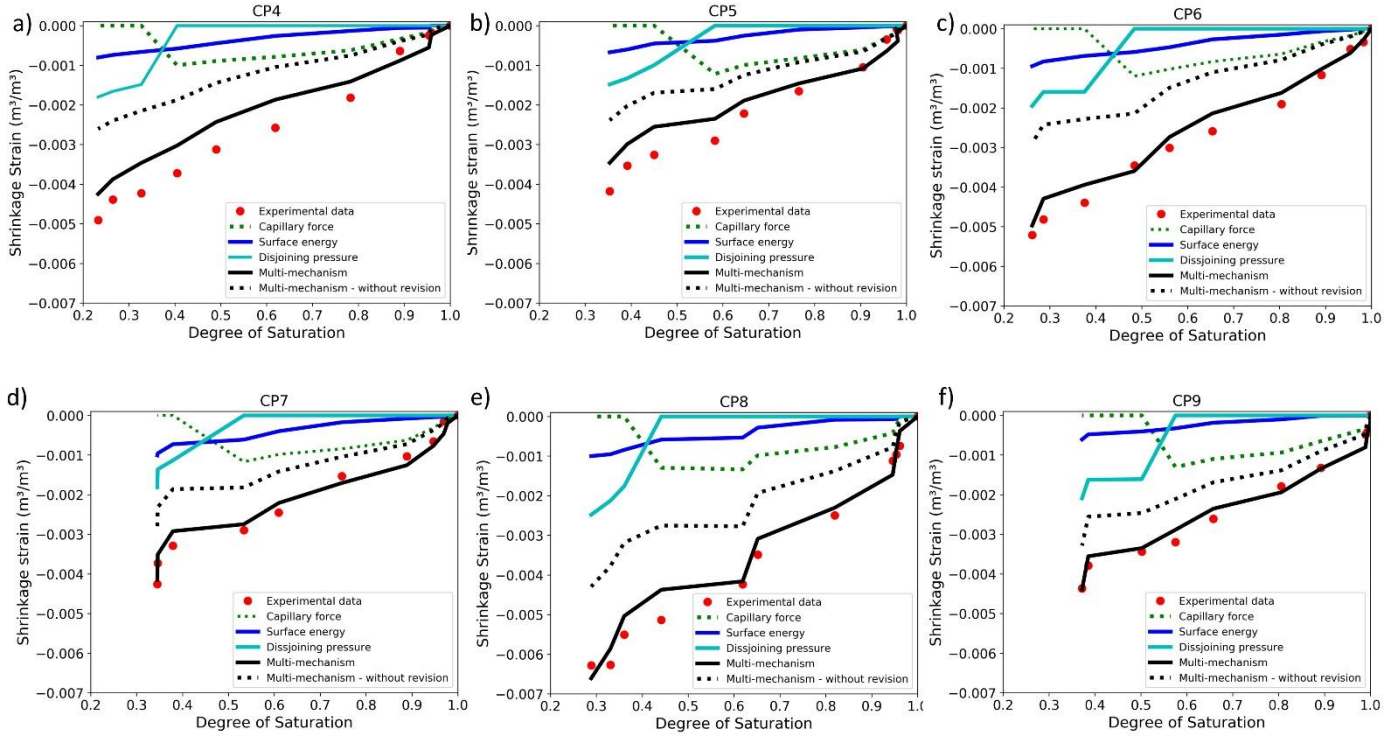

Figure 7. Contribution of each mechanism on predicted ultimate shrinkage vs experimental data for virgin materials. (multi-mechanism stands for proposed model plus experimental irreversible shrinkage)

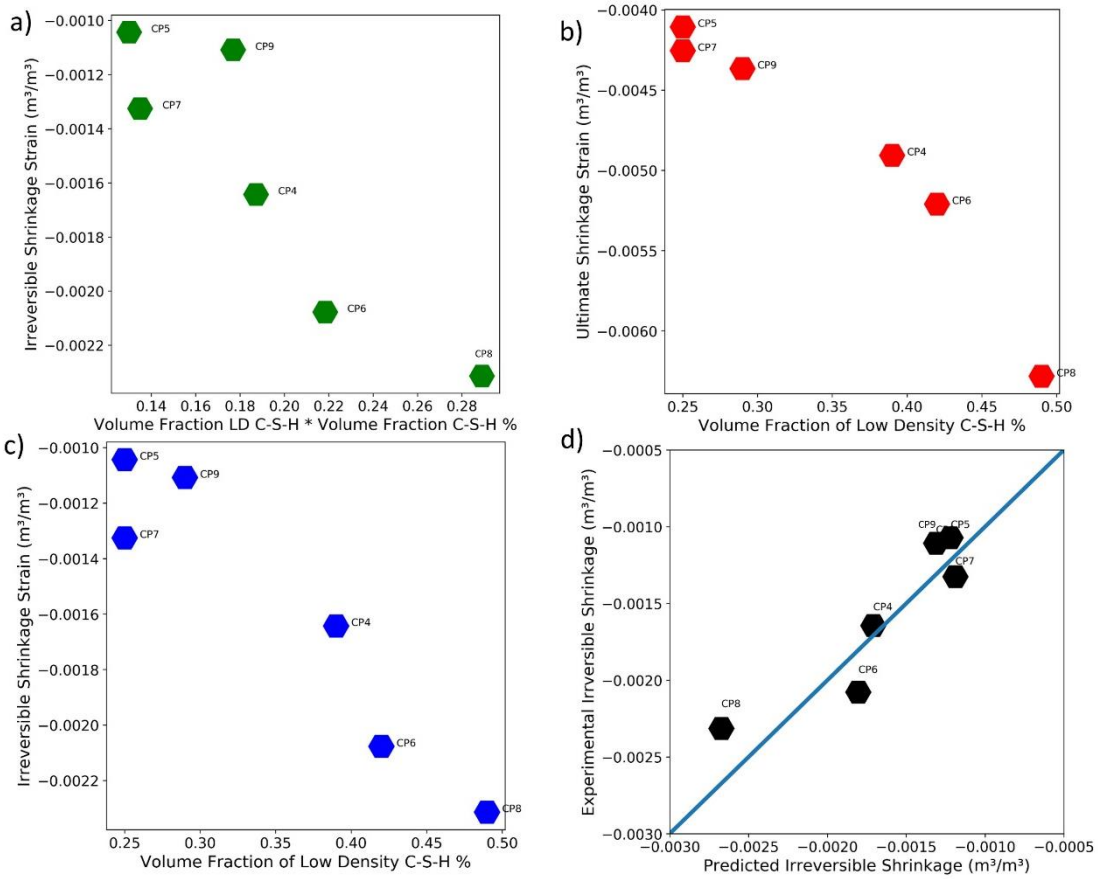

Figure 8. Irreversible shrinkage and its correlation with microstructural information.

1. Benboudjema, F., F. Meftah, and J.M. Torrenti, *A viscoelastic approach for the assessment of the drying shrinkage behaviour of cementitious materials.* Materials and Structures, 2006. **40**(2): p. 163.
2. Maruyama, I. and P. Lura, *Properties of early-age concrete relevant to cracking in massive concrete.* Cement and Concrete Research, 2019. **123**: p. 105770.
3. Craeye, B., et al., *Early age behaviour of concrete supercontainers for radioactive waste disposal.* Nuclear Engineering and Design, 2009. **239**(1): p. 23-35.
4. Craeye, B., et al., *Closure of the concrete supercontainer in hot cell under thermal load.* Nuclear Engineering and Design, 2011. **241**(5): p. 1352-1359.
5. J., B. and Bernier F., *Temperature Criterion Related to Clay Based Backfill Materials in the Framework of a Geological Repository of Heat Producing Radioactive Waste (HLW).* Proc. ICEM'Ol, The 8th International conference on Environmental Management, Bruges, Sept.30 - Oct.4, 2001.
6. *ACI-209 (2008), Guide for modeling and calculating shrinkage and creep in hardened concrete.* Farmington Hills, American Concrete Institute: p. 48.
7. *EN-1992-1-1 2008, Eurocode 2—design of concrete structures. Comite Europeen de Normalisation (CEN).* Brussels,: p. 259.
8. Bažant, Z.P. and S. Baweja, *Justification and refinements of model B3 for concrete creep and shrinkage 1. statistics and sensitivity.* Materials and Structures, 1995. **28**(7): p. 415-430.
9. Coussy, O., et al., *The equivalent pore pressure and the swelling and shrinkage of cement-based materials.* Materials and Structures, 2004. **37**(1): p. 15-20.
10. Xi, Y. and H.M. Jennings, *Shrinkage of cement paste and concrete modelled by a multiscale effective homogeneous theory.* Materials and Structures, 1997. **30**(6): p. 329.
11. Powers, T.C., *Mechanisms of Shrinkage and Reversible Creep of Hardened Cement Paste.* Conference Proceedings The Structure of Concrete, 1965.
12. Brochard, L., M. Vandamme, and R.J.M. Pellenq, *Poromechanics of microporous media.* Journal of the Mechanics and Physics of Solids, 2012. **60**(4): p. 606-622.
13. Vandamme, M., et al., *Modeling the Poromechanical Behavior of Microporousand Mesoporous Solids: Application to Coal*, in *Nonlinear Elasticity and Hysteresis*. 2014. p. 105-126.
14. Matthew B. Pinson, Enrico Masoero, and Hamlin M. Jennings, *Hysteresis from Multiscale Porosity: Modeling Water Sorption and Shrinkage in Cement Paste.* American Physical Society, 2015. **3**.
15. Luan, Y. and T. Ishida, *Enhanced Shrinkage Model Based on Early Age Hydration and Moisture Status in Pore Structure.* Journal of Advanced Concrete Technology, 2013. **11**(12): p. 360-373.
16. Nguyen, H., S. Rahimi-Aghdam, and Z.P. Bažant, *Unsaturated nanoporomechanics.* Proceedings of the National Academy of Sciences, 2020. **117**(7): p. 3440-3445.
17. POWERS, T.C., *The thermodynamics of volume change and creep.* Matériaux et Construction, 1968. **1**(6): p. 487–507.
18. Rezvani, M., T. Proske, and C.-A. Graubner, *Modelling the drying shrinkage of concrete made with limestone-rich cements.* Cement and Concrete Research, 2019. **115**: p. 160-175.
19. Vlahinić Ivan, Jennings Hamlin M., and Thomas Jeffrey J., *A constitutive model for drying of a partially saturated porous material.* Mechanics of Materials, 2009. **41**(3): p. 319-328.
20. Bishop, A.W., *The effective stress principle.* Teknisk Ukeblad 39, 1959: p. 859-863.
21. Babaei, S., et al., *A multiscale framework to estimate water sorption isotherms for OPC-based materials.* Cement and Concrete Composites, 2020. **105**: p. 103415.
22. Christensen, R.M., *Mechanics of Composite Materials.* Wiley-Interscience, New York,, 1979.
23. Christensen, R.M. and K.H. Lo, *Solutions for effective shear properties in three phase sphere and cylinder models.* Journal of the Mechanics and Physics of Solids, 1979. **27**(4): p. 315-330.
24. Biot, M.A., *Theory of Elasticity and Consolidation for a Porous Anisotropic Solid.* Journal of Applied Physics, 1955. **26**(2): p. 182-185.

25. Bangham, D.H. and R.I. Razouk, *The wetting of charcoal and the nature of the adsorbed phase formed from saturated vapours.* Transactions of the Faraday Society, 1937. **33**(0): p. 1463-1472.
26. Jennings H.M. and Tennis P.D., *A model for the developing microstructure in Portland cement pastes.* frAmer. Ceram. Soc, 1994. **77**(12): p. 3161-3172.
27. Hashin, Z., *Elastic moduli of heterogeneous materials.* Appl. Mech, 1962. **29**: p. 143–150.
28. Z. Hashin and S. Shtrikman, *A variational approach to the theory of the elastic behavior of multiphase materials.* J. Mech. Phys. Solids 1963. **11** p. 127–140.
29. W. Vichit-Vadakan and G.W. Scherer, *Measuring permeability of rigid materials by a beam-bending method: III. Cement paste.* Am. Ceram. Soc, 2002. **85**(6): p. 1537–44.
30. Z. Sun and G.W. Scherer, *Effect of air voids on salt scaling and internal freezing.* Cem. Concr. Res, 2010. **40**: p. 260–270.
31. Powers, T.C. and T.L. Brownyard, *Studies of the Physical Properties of Hardened Portland Cement Paste.* ACI Journal Proceedings. **43**(9).
32. Feldman, R.F. and P.J. SEREDA, *Sorption of water on compacts of bottle-hydrated cement. I. The sorption and length-change isotherms.* Journal of Applied Chemistry **14**(2): p. 87 - 93.
33. Feldman, R.F. and P.J. SEREDA, *SORPTION OF WATER ON COMPACTS OF BOTTLE-HYDRATED CEMENT. II* THERMODYNAMIC CONSIDERATIONS AND THEORY OF VOLUME CHANGE.* Journal of app Chem., February, 1964. **14**(2): p. 93-98.
34. HANSEN, W., *Drying Shrinkage Mechanisms in Portland Cement Paste.* Journal of the American Ceramic Society, 1987. **70**(5): p. 323-328.
35. Churaev, N.V., *The Relation between Colloid Stability and Wetting.* Journal of Colloid and Interface Science, 1995. **172**(2): p. 479-484.
36. Derjaguin, B.V., N.V. Churaev, and V.M. Muller, *Surface Forces.* Springer, Boston, MA, 1987.
37. Biot, M.A., *General Theory of Three-Dimensional Consolidation.* Journal of Applied Physics, 1941. **12**(2): p. 155-164.
38. Jennings, J.E.B. and J.B. Burland, *Limitations to the Use of Effective Stresses in Partly Saturated Soils.* Géotechnique, 1962. **12**(2): p. 125-144.
39. Nuth, M. and L. Laloui, *Effective stress concept in unsaturated soils: Clarification and validation of a unified framework.* International Journal for Numerical and Analytical Methods in Geomechanics, 2008. **32**(7): p. 771-801.
40. Mateusz Wyrzykowski, C.D.B., Pietro Lura, *Prediction of Drying Shrinkage of Cement-Based Mortars with Poroelastic Approaches - A Critical Review* Sixth Biot Conference on Poromechanics, Paris, France 2017. **6**: p. 579-586.
41. Maruyama, I., *Origin of Drying Shrinkage of Hardened Cement Paste: Hydration Pressure.* Journal of Advanced Concrete Technology 2010. **Vol. 8**(2): p. 187-200.
42. Ippei Maruyama, et al., *Microstructural and bulk property changes in hardened cement paste during the first drying process.* Cement and Concrete Research, 2014. **58**: p. 20–34.
43. Thomas Rougelot, Frédéric Skoczylas, and Nicolas Burlion, *Water desorption and shrinkage in mortars and cement pastes: Experimental study and poromechanical model.* Cement and Concrete Research, 2009. **39**: p. 36–44.
44. Galen Egan, et al., *Re-examining the influence of the inclusion characteristics on the drying shrinkage of cementitious composites.* Construction and Building Materials, 2017. **146**: p. 713-722.
45. Bullard J.W., *VCCTL Version 9.5 User Guide.* NIST, 2014.
46. Thomas J.J. and Jennings H.M., *A colloidal interpretation of chemical aging of the C-S-H gel and its effects on the properties of cement paste.* Cem Concr Res, 2006. **36**: p. 30-38.
47. Jennings H.M., et al., *A multi-technique investigation of the nanoporosity of cement paste.* Cem Concr Res, 2007. **37**: p. 329-336

48. Jennings, H.M., *Refinements to colloid model of C-S-H in cement: CM-II.* Cement and Concrete Research, 2008. **38**: p. 275–289.
49. Jennings, H.M., *A model for the microstructure of calcium silicate hydrate in cement paste.* Cement and Concrete Research, 2000. **30**: p. 101-116.
50. Hamlin M. Jennings, Aditya Kumar, and GauravSant, *Quantitative discrimination of the nano-pore-structure of cement paste during drying: New insights from water sorption isotherms.* Cement and Concrete Research 2015. **76**: p. 27-36.
51. Ippei Maruyama, et al., *Microstructural and bulk property changes in hardened cement paste during the first drying process.* Cement and Concrete Research, 2014. **58**: p. 20-34.
52. Ippei Maruyama, et al., *Microstructural changes in white Portland cement paste under the first drying process evaluated by WAXS, SAXS, and USAXS.* Cement and Concrete Research, 2017. **91**: p. 24-32.
53. Pinson, M., *Inferring Pore Size and Network Structure from Sorption Hysteresis.* 2014.
54. Babaei, S., et al., *Modeling of drying shrinkage in concrete : a multiscale poromechanics approach*, in *Symposium on Concrete Modelling : CONMOD2018, 26-29 August, 2018, Delft, the Netherlands*. 2018, RILEM Publications. p. 165-169.
55. Vlahinić, I., et al., *A novel and general form of effective stress in a partially saturated porous material: The influence of microstructure.* Mechanics of Materials, 2011. **43**(1): p. 25-35.
56. P. Acker, *Micromechanical analysis of creep and shrinkage mechanisms.* Creep, Shrinkage and Durability Mechanics of Concrete and other quasi-brittle Materials, 2001: p. 15-25.
57. Constantinides, G. and F.J. Ulm, *The effect of two types of C-S-H on the elasticity of cement-based materials: Results from nanoindentation and micromechanical modeling.* Cement and Concrete Research, 2004. **34**(1): p. 67-80.
58. Georgios Constantinides, *Invariant Mechanical Properties of Calcium-Silicate-Hydrates (C-S-H) in Cement-Based Materials: Instrumented Nanoindentation and Microporomechanical Modeling.* MASSACHUSETTS INSTITUTE OF TECHNOLOGY, 2006.
59. Ulm F.J., Constantinides G., and Heukamp F.H., *Is concrete a poromechanics material? – A multiscale investigation of poroelastic properties.* Mater Struct, 2004. **37**: p. 43-58.

Declaration of interests

☒ The authors declare that they have no known competing financial interests or personal relationships that could have appeared to influence the work reported in this paper.

☐The authors declare the following financial interests/personal relationships which may be considered as potential competing interests: